Solar-Terrestrial Physics. 2024. Vol. 10. Iss. 2. P. 74–92. DOI: 10.12737/stp-102202408. © 2024
T.D. Borisova, N.F. Blagoveshchenskaya, A.S. Kalishin, A.S. Kovalev. Published by INFRA-M Academic Publishing House

UDC 550.388.2
DOI: 10.12737/stp-102202408

Received October 25, 2023
Accepted February 29, 2024

DETERMINATION OF THE VECTOR VELOCITY OF ARTIFICIAL IONOSPHERIC IRREGULARITIES BASED ON DOPPLER MEASUREMENTS BY THE BISTATIC SCATTER METHOD OF HF RADIO SIGNALS PROPAGATING OVER LONG RADIO PATHS

T.D. Borisova
Arctic and Antarctic Research Institute, St. Petersburg, Russia, borisova@aari.ru

N.F. Blagoveshchenskaya
Arctic and Antarctic Research Institute, St. Petersburg, Russia, nataly@aari.nw.ru

A.S. Kalishin
Arctic and Antarctic Research Institute, St. Petersburg, Russia, askalishin@aari.ru

A.S. Kovalev
Arctic and Antarctic Research Institute, St. Petersburg, Russia, askovalev@aari.ru

Abstract. During experiments on the modification of the high-latitude ionosphere by high-power HF radio waves of ordinary or extraordinary polarization of the EISCAT/Heating facility (Tromsø, Norway) in 2013, 2016, and 2019, Doppler measurements of diagnostic HF radio signals over long radio paths were carried out by the bistatic scatter method. We studied characteristics of Doppler frequency variations in bistatic scattered radio signals, using the experimental results obtained along radio paths of different lengths (up to ~8500 km) and orientation. We examined numerical dependences of the Doppler frequency variations in a radio signal on the azimuth of the wave vector of a radio wave incident onto an artificially disturbed region, on the bistatic scattering angle, and on the azimuthal direction of irregularity motion in an artificially disturbed region of the ionosphere. From simultaneous measurements of the Doppler frequency f_D of the radio signal along two diagnostic radio paths, we numerically estimated the velocity vector of irregularities in the artificially disturbed region of the ionosphere. The total vector velocity of artificial ionospheric irregularities can be calculated from measurements of the Doppler frequency shift along several long diagnostic radio paths after preliminary analysis of experimental observations with the results of trajectory modeling of diagnostic HF radio signals.

Keywords: radio wave propagation, small-scale artificial ionospheric irregularities, Doppler observations, the EISCAT heating facility, modeling.

INTRODUCTION

When the ionosphere is modified by powerful short (HF) radio waves of ordinary (O-mode) or extraordinary (X-mode) polarization at altitudes close to the pump wave reflection, a number of irregularities are formed in ionospheric plasma, which cause significant changes in its parameters [Gurevich, 2007; Frolov, 2017; Blagoveshchenskaya, 2020; Fejer, 1979; Robinson, 1989]. On exposure to powerful HF radio waves at the pump frequency f_H of ordinary polarization, thermal (resonance) parametric instability (TPI) is excited [Grach, Trachtenhertz, 1975; Grach et al., 1977, 2016; Dimant, 1977; Vaskov, Gurevich, 1975, 1979; Erukhimov et al., 1987; Fejer, 1979]. The development of TPI gives rise to small-scale artificial ionospheric irregularities (SAIIs) of electron density along the geomagnetic field with a transverse size $l_\perp \leq \lambda 0 \approx 30 \div 100$ m (λ_0 is the wavelength of heating radio emission in vacuum). SAIIs are formed near the heights of the upper hybrid resonance of the pump wave h_{UH} for which the condition holds

$$f_H \approx f_{UH} = \sqrt{f_{pe}^2 + f_{ce}^2},$$

where f_{UH} is the upper hybrid resonance frequency, f_{ce} is the electron gyrofrequency.

In the ionosphere, an HF radio wave of ordinary polarization is reflected at a height at which the condition for the local plasma frequency f_{pe} is met $f_{pe}^2 = f_H (f_H - f_{ce})$. The X-mode pump wave reflection height is lower than the excitation heights of the upper hybrid f_{UH} oscillations; therefore, artificial irregularities during X-heating due to the development of thermal (resonance) parametric instability cannot be excited [Stubbe, Kopka, 1983; Robinson, 1989; Gurevich, 2007]. In experiments with the high-latitude EISCAT/Heating facility emitting an X-mode pump wave toward the magnetic zenith under quiet geomagnetic conditions, field-aligned SAIIs were first recorded [Blagoveshchenskaya et al., 2011]. In further experiments with the EISCAT/Heating facility using X-mode pump waves, a large volume of observational data on SAII generation was obtained. It has been established that in the high-latitude F-region of the ionosphere under X-heating, it is observed under weak geomagnetic activity when a powerful HF radio wave is emitted along the geomagnetic field (magnetic zenith) [Blagoveshchenskaya et al., 2018, 2019; Blagoveshchenskaya,

2020; Blagoveshchenskaya et al., 2022, 2023 and references therein]. Using CUTLASS (SuperDARN) radar measurements (Hankasalmi, Finland, 62.3° N, 26.6° E) [Greenwald et al., 1995; Lester et al., 2004], we have compared SAII characteristics and excitation parameters of the high-latitude ionosphere with dimensions transverse to the magnetic field $l_{\perp}$≈7.5÷12 m during O- and X-heating: depending on the ratio of the heating frequency f_H to the F2-layer critical frequency f_oF2; in the behavior of power levels P_{SAII} of bistatic scattered signals when the SAII generation mode passes from O- to X-heating; in a change of SAII rise times t_{rise} and relaxation times t_{rel}, taking into account the heating frequency f_H; the effect of transverse dimensions $l_{\perp}$ of scattering SAIIs during X-heating on disappearance/observation of SAIIs [Blagoveshchenskaya et al., 2018, 2019].

The possible generation of artificial ionospheric irregularities upon X-heating can be explained by the theory of generalized Rayleigh-Taylor instability [Kelley, 1989], which is excited in the presence of strong horizontal electron density gradients with an electric field of a powerful pump wave (X-mode) directed perpendicular to the magnetic field (electron density gradient) [Blagoveshchenskaya et al., 2023].

Ionospheric disturbances have a significant effect on propagation of electromagnetic waves in a wide frequency range. In the HF band, this effect leads, for example, to a change in the radio signal phase path and hence to a Doppler frequency shift. When HF radio signals propagate through an artificially disturbed region (ADR) of the ionosphere, filled with artificial irregularities, the effect of bistatic scattering is observed, first mentioned in [Thome, Blood, 1974]. Investigating the phenomenon of bistatic scattering of diagnostic HF radio signals by small-scale artificial ionospheric irregularities, produced by powerful HF radio waves of O-polarization, is an effective method of diagnosing and experimentally studying ionospheric irregularities [Namazov et al., 1975; Nasyrov, 1991; Afraimovich, 1982; Myasnikov et al., 2001; Uryadov et al., 2009; Frolov et al., 2012; Frolov, 2017; Gershman et al., 1984; Kalishin et al., 2021; Robinson, 1989; Yeoman et al., 1997; Frolov et al., 1997]. Experiments with heating facilities at high and middle latitudes of EISCAT/Heating facility (Tromsø) and SURA facility (Nizhny Novgorod) have revealed that the combination of HF heating of the ionosphere by O-polarization pump waves and Doppler measurements along diagnostic paths to 3000 km long is an effective method of studying and diagnosing SAIIs and medium-scale traveling ionospheric disturbances (TIDs) [Blagoveshchenskaya et al., 2006].

During bistatic scattering, motion of ionospheric irregularities causes a shift in the scattered signal frequency. In Doppler measurements at one diagnostic frequency f_{diagn}, we can determine the projection onto the direction of the scattering vector $\Delta\mathbf{k}=\mathbf{k}_s-\mathbf{k}_0$ (difference between wave vectors of incident $\mathbf{k}_0$ and scattered $\mathbf{k}_s$ HF radio waves) of the velocity of ionospheric irregularities V_k, moving in an artificially disturbed region of the ionosphere [Gershman et al., 1984]. SAII velocities during O-heating of the F-region according to measurements of diagnostic HF radio signals by the Doppler method along radio paths to 3000 km long have been estimated many times (e.g., [Belenov et al., 1977; Erukhimov et al., 1979; Nasyrov, 1991; Koloskov et al., 1999; Uryadov et al., 2004; Borisova et al., 2002]).

The SAII phase velocity and the plasma drift velocity were observed at a time in experiments [Eglitis et al., 1998] with simultaneous use of the EISCAT/Heating facility (Tromsø) [Rietveld et al., 2016], three-position incoherent scatter radars EISCAT UHF (European Incoherent SCATter Ultra High Frequency) in Tromsø, equipped with a transmitter and a receiver; radars in Kiruna and Sodankylä [Rishbeth, van Eyken, 1993], equipped only with receivers; as well as CUTLASS coherent HF radars in Hankasalmi (Finland) and Pikkvibaer (Iceland) [Greenwald et al., 1995]. A good correspondence has been established between the observed phase velocities of irregularities, generated by the heating facility, and the plasma drift velocity component in the CUTLASS radar line of sight. Plasma drift velocities as measured by EISCAT UHF incoherent scatter radars [Eglitis et al., 1998] varied from 20 to 270 m/s, sometimes there were velocities higher than 500–700 m/s.

In [Belenov et al., 1977; Avdeev et al., 1994], the total SAII drift velocity vector is estimated from measurements of the Doppler shift in bistatic scattered radio signals at spaced reception along mutually orthogonal diagnostic radio paths. Calculation methods have been developed in [Blagoveshchenskaya et al., 2006; Borisova et al., 2007; Vertogradov et al., 2015]. The calculation results were compared with three-position measurements of the phase velocity of ionospheric plasma by EISCAT incoherent scatter radars [Borisova et al., 2007]. During heating cycles (November 19, 2003) of powerful HF radio wave emission by the EISCAT/Heating facility, SAIIs were formed at 220–250 km. Plasma drift was measured by EISCAT radars at 160–170 km. A satisfactory correspondence was obtained between SAII motion directions in the F-region, calculated from Doppler HF and EISCAT radar measurements. Differences between azimuthal directions were 4–15 and 15–30 %, and the large deviations of the values can be explained by different heights of measurements in the ionosphere.

The purpose of this work is to determine the velocity vector of SAIIs, caused by the influence of powerful HF radio waves of O- or X-polarization on the high-latitude F-region, from experimental data. We have used multichannel Doppler HF measurements performed during experiments with the EISCAT/Heating facility in February 2013, October 2016, and October 2019.

As a result of the research we 1) have examined the features of the behavior of SAIIs, produced by powerful HF radio emission of O- or X-polarization (rise and relaxation times of SAIIs, features of SAII evolution), from Doppler observations over long diagnostic radio paths and have compared with the SAII characteristics derived from CUTLASS radar observations; 2) have simulated the trajectory characteristics of diagnostic HF radio signal propagation over long bistatic scattering

paths transmitter — artificially disturbed region (ADR) of the ionosphere — receiver; 3) have calculated SAII velocities from Doppler measurements of diagnostic HF radio signals over long diagnostic radio paths during heating experiments.

1. OBSERVATION FACILITIES AND METHODS

Experiments on the impact of powerful HF radio waves of O- or X-polarization were carried out with the EISCAT/Heating facility, located in Norway near Tromsø (69.6° N, 19.2° E, *L*=6.2) [Rietveld et al., 2016], on February 25, 2013, October 20, 2016, and October 21, 2019

Artificial ionospheric irregularities over Tromsø were observed along diagnostic radio paths, using the method of bistatic scattering of diagnostic HF radio signals by a multichannel Doppler equipment [Kalishin et al., 2021]. Table 1 lists characteristics of the diagnostic radio paths: names and geographic coordinates of receiver and transmitter, frequency of radiation transmitters f_{diagn}, length of diagnostic paths (transmitter—receiver (direct path); transmitter—ADR over Tromsø; ADR— receiver and transmitter—ADR—receiver (bistatic scattering path)).

Diagnostic HF radio signals were recorded at NIS Gorkovskaya near St. Petersburg on October 20, 2016 and October 21, 2019 and in St. Petersburg and Lovozero on February 25, 2013.

A map explaining the geometry of the 2013, 2016, and 2019 experiments is given in Figure 1.

A powerful HF radio wave of O-polarization on February 25, 2013 was emitted in the morning at a frequency f_H=5.423 MHz toward the magnetic zenith in the 10-min heating/5-min pause mode. The SAII excitation was recorded from 08:30 to 09:15 UT

Table 1

Characteristics of diagnostic HF radio paths: names and geographic coordinates of receiver and transmitter, frequency of diagnostic transmitters, length of diagnostic paths (transmitter—receiver, transmitter—ADR, transmitter—ADR—receiver).

Receiver latitude, longitude	Transmitter latitude, longitude	f_{diagn}, MHz	Path transmitter—receiver, *D*, km	Path Transmitter—ADR, *D*, km	Path ADR—receiver *D*, km	Path PP transmitter—ADR—receiver *D*, km
Gorkovskaya station (near St. Petersburg) 59.9° N; 30.3° E	Nashville 36.2° N; –86.9° W.	13.845 15.825	7850	6830	1150	7980
	Hialeah Gardens 25.9° N; –80.37° W	15.770 21.675	8570	7662	1150	8810
	Irkutsk 52° N; 104° E	21.800	4380	4515	1150	5660
Lovozero 68° N; 35° E	Moscow 55.7° N; 37.6° E	12.075	1370	1800	670	2470

For transmitters located in Nashville and Hialeah Gardens, (hereinafter — located in America).

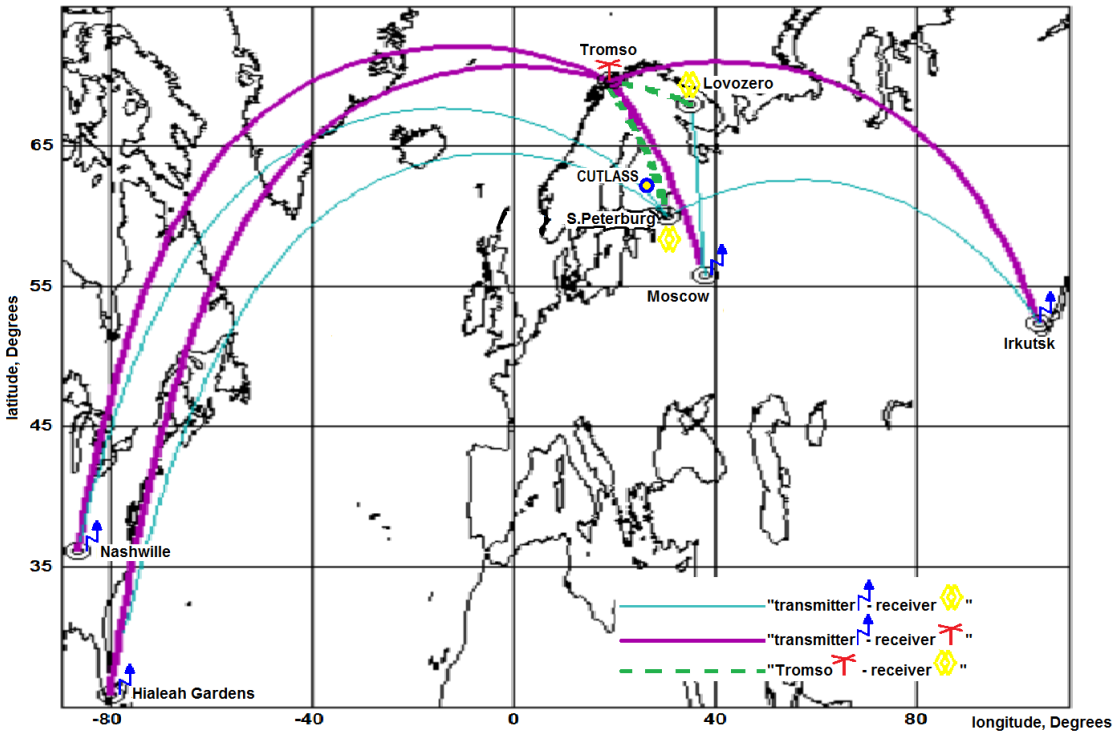

Figure 1. Geometry of experiments

(LT=UT+2 hrs) by the bistatic scatter method along two diagnostic paths equipped with transmitters and receivers at different stations: Irkutsk — Tromsø — St. Petersburg (f_{diagn}=21.8 MHz) and Moscow —Tromsø — Lovozero (f_{diagn}=12.075 MHz).

On October 21, 2019, EISCAT/Heating emitted at f_H=4.2 MHz with O-polarization at 15:00–15:34 UT and X-polarization at 15:35–15:48 UT toward the magnetic zenith (LT=UT+1 hr). The emission cycles were 3-min heating / 2-min pause. In St. Petersburg, simultaneous measurements were performed by the bistatic scatter method along the diagnostic HF paths Hialeah Gardens — Tromsø — St. Petersburg (f_{diagn}=15.770 MHz); Nashville — Tromsø — St. Petersburg (f_{diagn}=15.825 and f_{diagn}=13.845 MHz), whose transmitters are located in North America.

On October 20, 2016, EISCAT/Heating emitted at f_H=4.543 MHz with O- or X-mode from 14:16 to 16:00 UT (LT=UT+1 hr). SAII excitation in this experiment was recorded simultaneously by the CUTLASS HF radar and the method of bistatic scattering of diagnostic HF radio signals in St. Petersburg. Doppler observations were made along the Hialeah Gardens — Tromsø — St. Petersburg path (f_{diagn}=17.750 and f_{diagn}=21.675 MHz).

2. OBSERVATIONAL RESULTS

2.1. October 20, 2016 experiment

The ionosphere in the October 20, 2016 experiment was modified by the EISCAT/Heating facility under quiet geomagnetic conditions and low solar activity (three-hour magnetic activity index K_p=0, Wolf number W=31). During the experiment, the F2-layer critical frequencies f_oF2 and f_xF2 (ordinary and extraordinary polarization), as observed at the vertical sounding (VS) station in Tromsø, gradually decreased from 5.5 and 6.2 MHz at 14:15 UT to 4.5 and 5.2 MHz at 15:30 UT (LT=UT+ 1 hr) and then before 16:00 UT f_oF2 and f_xF2 decreased to 4.1 and 4.8 MHz.

From 14:15 to 16:00 UT, a powerful HF radio wave of the EISCAT/Heating facility at f_H=4.543 MHz of ordinary or extraordinary polarization was emitted toward the magnetic zenith by phased array antenna No. 2 (PAA-2) with a beamwidth of ~15° (at the level of 3 dB), providing an effective transmitter power P_{eff}=150 MW. At 14:15–14:30 UT, the emission was implemented with the O-mode; at 14:30–16:00 UT, with the X-mode. The transmitter operated in cycles of 10-min heating — 5-min pause. Before 15:30 UT, the pump frequency was lower than the F2-layer critical frequency (ordinary polarization), $f_H<f_o$F2. After 15:30 UT, the heating was performed under conditions $f_H>f_o$F2 and $f_H<f_x$F2.

The SAII characteristics were measured by the CUTLASS HF radar on October 20, 2016 in a non-standard mode [Lester et al., 2004]. The CUTLASS radar transmitted to a narrow-beam antenna in a stereo mode with a beam width of ~3.3°, oriented to an artificially disturbed region of the ionosphere over Tromsø (beam 5) at three frequencies ranging from 10 to 20 MHz. The time resolution of the measurements was 3 s, the resolution for the "gate" range was 15 km, the first gate beginning from 480 km. The frequency range of the CUTLASS radar transmission was 8–20 MHz, so SAIIs with transverse scales 7.5–18.75 m can be observed.

Study and analysis of SAII measurement data based on CUTLASS radar measurements in the October 20, 2016 experiment have been published in [Blagoveshchenskaya et al., 2018]. In this study, we compare the characteristics of SAII development, using the results of their simultaneous recording by the CUTLASS radar and by the method of bistatic scattering of diagnostic HF radio signals over long paths.

The SAII characteristics were measured by the method of bistatic scattering of diagnostic HF radio signals at the NIS station Gorkovskaya along the Hialeah Gardens—Tromsø—St. Petersburg path at two diagnostic frequencies f_{diagn}= 17.750 and 21.675 MHz on October 20, 2016. The results of the SAII observation by the bistatic scatter method for long radio paths in experiments with X-heating have not been presented before.

Figure 2 presents the results of SAII observations by the CUTLASS radar and by the bistatic scatter method on October 20, 2016 at 14:15–16:00 UT to compare SAII parameters measured by different methods during heating cycles.

Figures 2, *a*, *b*1–*b*3 show radar measurement data taken from [Blagoveshchenskaya et al., 2018]. Heating cycles and polarization of the pump frequency f_H are indicated on the time axis. The averaged powers of signals scattered by SAIIs P_{SAII} in the artificially disturbed region (ADR) of the ionosphere at three frequencies of 12.4, 13.3, and 16.3 MHz, shown in Figure 2, *a*, reveal a cycle-to-cycle variation in $P_{SAII}(t)$ throughout the observation period. Figure 2, *b*1–*b*3 illustrates motions of P_{SAII} depending on range (range gate) and time UT at three frequencies of 12.4, 13.3, and 16.3 MHz corresponding to backscattering from SAIIs with transverse scales $l_\perp$ from 12.1 to 9.2 m. The signals scattered by SAIIs were recorded in the range gate 780–1080 km corresponding to measurements in gate numbers from 20 to 40. The results of the CUTLASS radar measurements allow us to estimate spatial dimensions of ADR in the ionosphere D_{ADR} in the direction of the radar beam. For O-heating cycles, D_{ADR} varies from 180 km for SAII with a scale $l_\perp$~9.2 m to 165 km for $l_\perp$~12.1 m. At X-heating (in the first cycle after O-heating), D_{ADR}~150 km for $l_\perp$~9.2 m and D_{ADR}~120 km for $l_\perp$~12.1 m. In subsequent X-heating cycles, D_{ADR} increases.

The minimum transverse size of SAIIs responsible for bistatic scattering of radio waves is determined by the expression [Erukhimov et al., 1979; Nasyrov, 1991]

$$l_\perp=\lambda/2\sin(\theta/2), \quad (1)$$

where $\lambda=f_{diagn}/c$ is the wavelength of a diagnostic HF radio wave; θ is the bistatic scattering angle between wave vectors of incident $\mathbf{k}_0$ onto SAII and scattered $\mathbf{k}_s$ by waves; c is the speed of light. Calculated $l_\perp$ and θ for the experimental conditions presented in this paper are

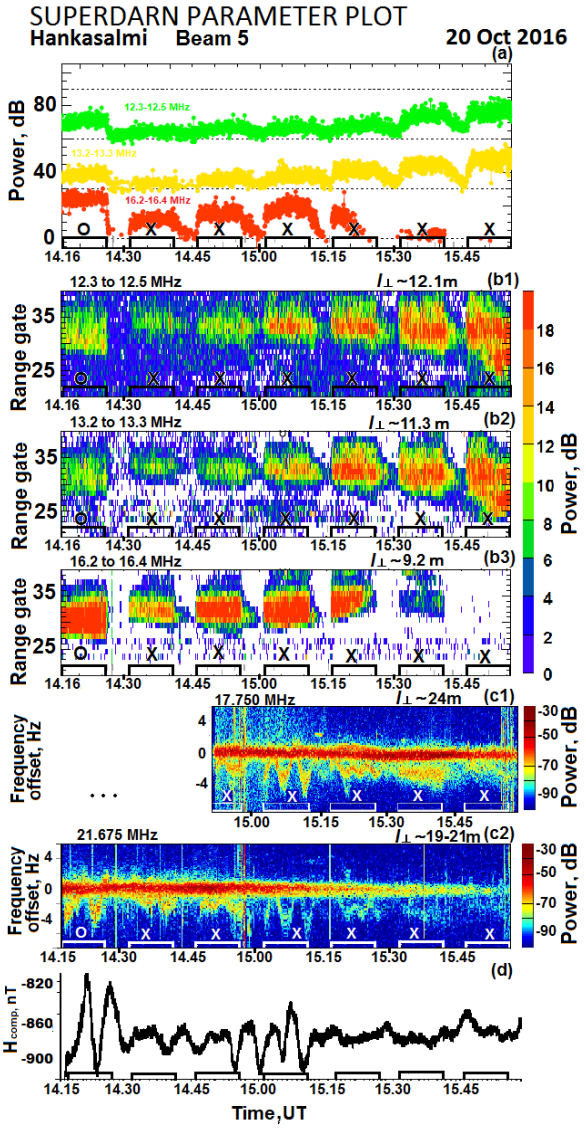

Figure 2. Observations (*a*, *b*1–*b*3) with the CUTLASS coherent Doppler HF radar in Hankasalmi, Finland (beam 5 aimed at an artificially disturbed region of the ionosphere above Tromsø); measurements (*c*1, *c*2) by the method of bistatic scattering of diagnostic HF radio signals (sonograms) along the Hialeah Gardens—Tromsø—St. Petersburg path, f_{diagn}=17.750 and 21.675 MHz; *H* is the geomagnetic field component (*d*) of the magnetovariation station Tromsø. Heating cycles and the powerful HF radio wave polarization in use are indicated on the time axis of the bottom panel

listed in Table 2; formulas for the calculations are presented in Section 3.2. Figure 2, *c*1, *c*2 exhibits dynamic Doppler spectra (sonograms) of diagnostic HF radio signals along the Hialeah Gardens—Tromsø—St. Petersburg path, f_{diagn}=17.750 MHz and 21.675 MHz, measured on October 20, 2016 by the method of bistatic scattering of diagnostic HF radio signals simultaneously with observations made by the CUTLASS radar. Also shown are minimum transverse dimensions of scattering SAIIs $l_\perp$=24 and 19–21 m for 17.750 and 21.675 MHz respectively, calculated from (1), taking into account bistatic scattering angles of diagnostic radio signals in ADR over Tromsø for experimental conditions on October 20, 2016 (see Table 2). The zero Doppler frequency shift f_D=0 corresponds to measurements of diagnostic HF radio signals propagating from a transmitter to a receiver along the great-circle arc (direct signal) over the Hialeah Gardens—St. Petersburg path. Figure 2, *c*1, *c*2 indicates that during the measurement period in all cycles of O- and X-heating bistatic scattered signals moving from zero mainly to the negative part of the Doppler spectrum and forming f_D tracks in sonograms were recorded. Doppler measurements detect the structure of SAII behavior in a heating cycle. There were wave variations in the behavior of the Doppler frequency f_D with 2–3.5 min periods, which coincided with the periods of oscillations of the magnetic field *H* component (Figure 2, *d*), measured by the magnetovariation station Tromsø [https://flux.phys.uit.no/ArcMag/].

Table 3 presents some SAII characteristics measured by the CUTLASS radar and by the method of bistatic scattering of diagnostic HF radio signals over a long radio path on October 20, 2016 during a heating experiment with the EISCAT/Heating facility.

Comparison between characteristics of SAIIs generated by a powerful radio wave with X-mode polarization of the EISCAT/Heating facility on October 20, 2016, simultaneously measured by the CUTLASS HF radar and by the bistatic scatter method (see Figure 2 and Table 3), has shown correspondence between SAII excitation and development, as well as close values of the following SAII parameters.

- During X-heating, SAII rise times had the same value t_{rise}<30 s.
- The relaxation time of bistatic scattered signals coincided and had values t_{rel}=60–120 s for $f_H<f_o$F2 and t_{rel}~120-180 s for $f_H>f_o$F2 and $f_H<f_x$F2.
- There was a similar characteristic change in the power levels P_{SAII} of bistatic scattered signals during the transition of the SAII generation mode from O- to X-heating, as well as a decrease in P_{SAII} in the first X-heating cycle after O-heating and an increase in P_{SAII} in subsequent cycles.
- A characteristic feature of SAII disappearance/observation at $f_H>f_o$F2 and $f_H<f_x$F2 depending on transverse dimensions $l_\perp$ of scattering irregularities is observed during X-heating. First, irregularities with smaller dimensions $l_\perp$ disappear. At 15:30 UT, SAIIs with $l_\perp$~9.2 m begin to disappear.

Note that backscattering (θ=180°) at f_{diagn}=17.750 and 21.675 MHz occurs by SAIIs with transverse dimensions $l_\perp$~6.9 and 8.4 m. Diagnostic HF radio signals with f_{diagn}=17.750 and 21.675 MHz were recorded up to 16 UT on October 20, 2016. Scattering of radio signals at these frequencies occurred by SAIIs with much larger dimensions $l_\perp$~19–20 and 24 m respectively (see Table 2). This fact is consistent with the established patterns of SAII disappearance during X-heating at $f_H>f_o$F *2* and $f_H<f_x$F*2* depending on $l_\perp$, as inferred from CUTLASS radar data [Blagoveshchenskaya et al., 2018].

Simultaneous observations of SAIIs on October 20, 2016 by the CUTLASS radar and by the bistatic scatter method have demonstrated the same characteristics of

Table 2

Calculated values of scattering angles θ and transverse dimensions of ionospheric irregularities $l_\perp$ scattering diagnostic signals with f_{diagn} along the paths under study and the azimuth of the difference vector $\Delta\mathbf{k}=\mathbf{k}_0-\mathbf{k}_s$ in 2016, 2019, and 2013 experiments.

Transmitter	Receiver	$f_{diagn,}$ MHz	$l_\perp$, m in view of Θ	Θ, deg for experimental conditions	Azimuth of the difference vector $\Delta\mathbf{k}$	ΔAz_{k0}, deg
C	C	12.400	12.10	180		
Moscow	Lovozero	12.075	13.80	134	138	±5
C	C	13.300	11.28	180		
Nashville	S.Pb	13.845	21–22	30	42	±2.5
Hialeah Gardens	S.Pb	15.770	27–28	40	38	±2.5
Nashville	S.Pb	15.825	18–19	30	42	±2.5
C	C	16.300	9.20	180		
C	C	16.600	9.04	180		
Hialeah Gardens	S.Pb	17.750	24	40	38	±2.5
Hialeah Gardens	S.Pb	21.675	19–21	40	38	±2.5
Irkutsk	S.Pb	21.800	7.00	102	108	±3

C denotes a transmitter and a receiver of the Doppler HF radar CUTLASS

Table 3

SAII characteristics measured by the CUTLASS radar and by the bistatic scatter method along the Hialeah Gardens — Tromsø — St. Petersburg radio path at diagnostic frequencies f_{diagn}=17.750 MHz and f_{diagn}=21.675 MHz on October 20, 2016 during O- and X-heating from 14:16 to 16:00 UT.

Time, relation between f_H, f_oF2, and f_xF2	CUTLASS radar observations	Doppler measurements
14:16–14:26 UT (LT=UT+1 hr) O-heating, $f_H<f_o$F2	SAII generation The rise time t_{rise} of bistatic scattered signals for the O-heating cycle is not determined due to technical problems. The relaxation time of bistatic scattered signals t_{rel}<30 s.	SAII generation (according to f_{diagn}=21.675 MHz) with t_{rise}<30 s, t_{rel} is not determined due to the overlap of f_D of outshifted and main tracks.
14:31–16:00 UT X-heating; before 15:30 UT $f_H<f_o$F2, after 15:30 UT $f_H>f_o$F2 and $f_H<f_x$F2	SAII generation At X-heating, t_{rise}<30 s.	SAII generation with t_{rise}<30 s.
14:31–14:41 UT first X-heating cycle after O-heating $f_H<f_o$F2	A decrease in P_{SAII} by 4–15 dB and a decrease in D_{ADR}.	A decrease in P_{SAII} by 10 dB for f_{diagn}=21.675 MHz. D_{ADR} is not determined from Doppler measurements.
14:31–15:30 UT X-heating as f_H approaches f_oF2, $f_H<f_o$F2 and $f_H<f_x$F2	P_{SAII} increases (on average) by ~10–12 dB per period.	Direct signal power level P_{DS} of an HF radio wave has an effect on a change in P_{SAII} (*). For f_{diagn}=17.750 MHz, the levels of P_{DS} and P_{SAII} do not change until 15:41 UT. For f_{diagn}=21.675 MHz, the levels of P_{DS} and P_{SAII} remain unchanged until 14:56 UT. After 15:01 UT, with a decrease in P_{DS} by 20 dB, P_{SAII} decreases by 10–15 dB
	Relaxation time of bistatic scattered signals t_{rel}~60–120 s.	t_{rel}~60–120 s.
15:31–16:00 UT, X-heating $f_H>f_o$F2 and $f_H<f_x$F2	First, SAIIs with smaller scales weaken and then disappear ($l_\perp$=9.2 m, Figure 2, *a* and *b3*), but P_{SAII} and $D_{ADR\ increase.}$ Larger-scale SAIIs ($l_\perp$=11.3 and 12.1 m)	SAIIs with $l_\perp$~19–20 and 24 m (Table 3) were recorded before 16 UT. For f_{diagn}=17.750 MHz, a decrease in P_{SAII} by 15 dB is observed with a decrease in P_{DS} by 30 dB and for f_{diagn}=21.675 MHz. P_{SAII} decreases by 10 dB with a 20 dB decrease in P_{DS}.
	t_{rel}~120–180 s.	t_{rel}~120–180 s

The decrease in the power levels of direct P_{DS} and scattered P_{SAII} signals at f_{diagn}=21.675 MHz (Figure 2, *c2*) after 15:10 UT is explained by a change in the number of jumps of the propagation trajectory of diagnostic signals over a long path crossing seven time zones in the noon—dusk direction. Regular diurnal variations of the F2-layer parameters in the distribution of the ionosphere along the path (a decrease in the electron density N_e and an increase in the height of the F2-layer maximum h_mF2) lead to an increase in the number of jumps and hence to a decrease in the power of radio signals incident on ADR in the ionosphere over Tromsø and received in St. Petersburg (see Section 3).

the behavior of SAIIs, generated by powerful HF radio emission with X-mode such as rise and relaxation times of P_{SAII}, the temporal behavior of P_{SAII} depending on the relation of f_H, f_oF2, and f_xF2.

Recording of HF radio signals, bistatically scatted by SAIIs excited by the EISCAT/Heating facility, from American transmitters in St. Petersburg allows us to detect SAIIs with transverse dimensions $l_\perp$ 2–3 times larger than at the same diagnostic frequencies of transmitters from Europe or Asia due to the bistatic scattering angle <40°.

2.2. October 21, 2019 experiment

On October 21, 2019 at f_H=4.2 MHz, the EISCAT/Heating facility emitted pump waves of ordinary polarization at 15:00–15:34 UT and extraordinary polarization at 15.35–15.48 UT (LT=UT+1 hr) toward the magnetic zenith. Emission cycles are 3-min heating — 2-min pause. In the experiments, PAA-2 was employed with a beamwidth of ~15° (at 3 dB). The effective power of the facility P_{eff}~200 MW. The electric field strength of a pump wave at 200–220 km E~0.6–0.67 V/m. Experimental threshold values of the electric field strength E of EISCAT/Heating facility pump waves required to generate SAIIs E~0.29 V/m for O-mode and E~0.53–0.6 V/m for X-mode [Borisova et al., 2017], thus the level of radiated energy in the ionosphere is sufficient to generate SAIIs. The ADR transverse size determined from the threshold power of the HF radio wave from the heating facility was ~50 km for X-heating and ~ 90 km for O-heating. The experiment was performed during low solar and quiet magnetic activity (W=0, K_p=1). Critical frequencies f_oF2 at 15–16 UT, according to the data from the vertical sounding ionosonde in Tromsø, varied from 4.3 MHz to 4.0 MHz. For the pump frequency f_H of a powerful HF radio wave in the O-mode, the conditions $f_H \le f_o$F2 held, and when switching the pump wave polarization to the X-mode the conditions f_oF2<f_H<f_xF2 were met, where f_oF2 and f_xF2 are the F2-layer critical frequencies of ordinary and extraordinary components. Accordingly, under the conditions considered SAIIs can be generated both during O- and X-heating of the high-latitude F-region over the EISCAT/Heating facility.

From 15:20 to 15:50 UT, Doppler measurements were carried out of diagnostic HF radio signals propagating along the paths Nashville—Tromsø—St. Petersburg at two frequencies f_{diagn}=13.845 and 15.825 MHz and Hialeah Gardens—Tromsø—St. Petersburg at f_{diagn}=15.770 MHz (see Figure 1, Table 1).

Figure 3 presents sonograms of diagnostic HF radio signals measured on October 21, 2019 from 15:18 to 15:58 UT along the paths Nashville—Tromsø—St. Petersburg, f_{diagn}=15.825 MHz (Figure 3, *a*) and f_{diagn}=13.845 MHz (Figure 3, *c*), and Hialeah Gardens—Tromsø—St. Petersburg, f_{diagn}=15.770 MHz (Figure 3, *b*), the diagnostic frequency f_{diagn}, and the minimum transverse size $l_\perp$ of scattering SAIIs calculated for experimental conditions on October 21, 2019 (see Table 3).

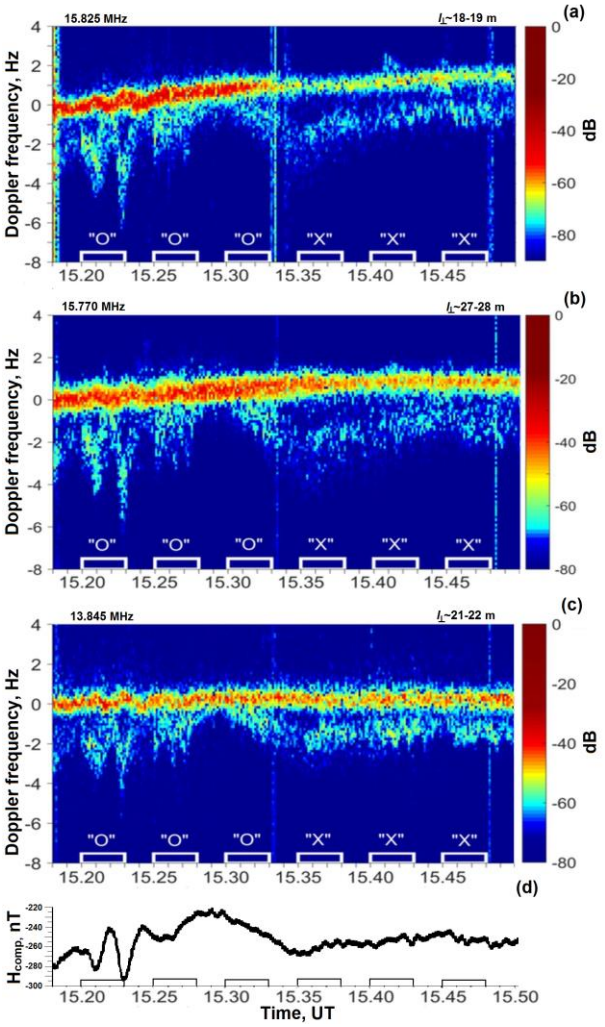

Figure 3. Sonograms of diagnostic HF radio signals during the October 21, 2019 heating experiment: the Nashville—Tromsø—St. Petersburg path, f_{diagn}=15.825 MHz (*a*) and f_{diagn}=13.845 MHz (*c*); the Hialeah Gardens—Tromsø—St. Petersburg path, f_{diagn}=15.77 MHz (*b*); the geomagnetic field H component of the magnetovariation station Tromsø (*d*). Operation intervals of the heating facility and pump wave polarization are indicated

Heating cycles and polarization of the pump wave frequency f_H are indicated on time axes. The zero Doppler frequency shift f_D=0 corresponds to a direct signal. Interference in sonograms in the form of vertical stripes at 15:33:30 and 15:48:30 UT is associated with the operation of oblique chirp signal and vertical ionospheric sounding transmitters located directly on the territory of NIS Gorkovskaya near the multichannel Doppler equipment. During operation cycles of the EISCAT/Heating facility's transmitter, bistatic scattered signals at f_D shifted to the negative side of the Doppler spectrum were recorded over all diagnostic radio paths. In sonograms, Doppler scattered signals formed tracks with a spectral scattering width 1.5–2.5 Hz and wave variations in $f_D(t)$ with 2–3 and 14 min periods. The periods of f_D oscillations coincided with the periods of magnetic field H-

component oscillations measured by the magnetovariation station Tromsø [https://flux.phys.uit.no/ArcMag /] (Figure 3, *d*).

In general, there is one track of f_D(t) in the sonograms. Variations in f_D(t) correlate along the three diagnostic paths. This fact suggests that HF radio signals at three frequencies are scattered by SAIIs of one spatial ionospheric region disturbed by EISCAT/Heating powerful HF radio emission. Figure 3 shows a decrease in the power of direct signals P_{DS} near zero frequency and bistatic scattered P_{SAII} at outshifted frequencies f_D for a signal from Nashville, f_{diagn}=15.825 MHz, after 15:33 UT (see Figure 3, *a*), and for a radio signal from Hialeah Gardens's transmitter, f_{diagn}=15.770 MHz, after 15:37 UT (see Figure 3, *b*) (it is explained by an increase in jumps in propagation trajectories of diagnostic HF radio signals during the day over the paths crossing seven time zones in the noon—dusk direction, see Figure 5). At f_{diagn}=13.845 MHz, the number of propagation trajectory jumps remains unchanged until 16:00 UT.

According to Doppler measurements on October 21, 2019, the parameters of the behavior of bistatic scattered signals by SAIIs generated in heating cycles were recorded over long paths.

Rise times of P_{SAII} from the beginning of the heating cycle on October 21, 2019 t_{rise}~10 s when the O-mode pump frequency f_H was emitted and t_{rise}≥30 s when the X-mode pump wave was used.

During the first X-heating cycle at 15:35–15:38 UT (after the O-heating cycle), under conditions $f_H>f_oF2$ and $f_H<f_xF2$, bistatic scattered signals reached maximum power in t_{rise}~40–50 s after the beginning of emission. During subsequent X-heating cycles in the presence of weak bistatic scattered signals during pauses, P_{SAII} increased earlier — in 30–50 s after the start of the heating cycle.

According to Doppler measurements of $f_D(t)$ at f_{diagn}=13.845 MHz during the O-heating cycle at 15:30–15:33 UT and during subsequent X-heating cycles at 15:35–15:38 UT and 15:40–15:43 UT, power levels of bistatic scattered signals P_{SAII_O}=–48 dB; P_{SAII_X}=–55 dB and P_{SAII_X}=–50 dB respectively were observed (see Figure 3, *c*). Variations in P_{SAII} for f_{diagn}=15.825 MHz for the three cycles P_{SAII_O}=–63 dB, P_{SAII_X}=–75 dB, and P_{SAII_X}=–65 dB (see Figure 3, *a*).

Thus, we can see a decrease in the power of bistatic scattered signals P_{SAII} when switching the pump wave emission mode from O-mode to X-mode during the first cycle and an increase in P_{SAII} during the subsequent X-heating cycle (conditions of constant P_{DS} level during X-heating were selected).

With the start of the transmitter emission during X-heating cycles, P_{SAII} exceeds the natural noise level in t_{rise}. Further during the heating cycle, P_{SAII} continues to increase to a certain maximum level. During the X-heating cycle, P_{SAII} varies a lot. Depending on the duration of the cycle period, several maxima of P_{SAII} may be recorded.

At outshifted frequencies $f_D(t)$ on October 21, 2019 (see Figure 3), the relaxation time of artificial irregularities after the end of the X-heating cycles t_{rel}~120 s. The relaxation time of the irregularities on this day was limited to the duration of the pauses between transmitter emissions.

Consequently, according to Doppler measurements during X-heating the SAII parameters were observed which coincided with those recorded by the CUTLASS radar:

- increased t_{rise} and t_{rel};
- the characteristic behavior of $P_{SAII}(t)$ when switching from O-heating to X-heating and further in subsequent heating cycles.

That day, an increased relaxation time of P_{SAII} was also recorded, and after the end of O-heating cycles t_{rel}=60–100 s. In [Yampolskii, 1989; Nasyrov, 1991; Blagoveshchenskaya et al., 2007; Frolov et al., 2008; Hysell et al., 1996], the relaxation time of artificial irregularities excited by an O-mode pump wave from the SURA heating facility was studied. According to measurements of diagnostic HF signals scattered by artificial irregularities (with transverse dimensions from a few meters to several kilometers), after switching off the ionosphere heating transmitter, the presence of two SAII relaxation stages was recorded — the so-called rapid relaxation lasting for 10–20 s and slow relaxation lasting to several minutes. Effects of bistatic scattering of diagnostic HF signals on ionospheric irregularities with scales $l_\perp$~8÷20 m whose diffusion explains the rapid relaxation of SAIIs were examined. The slow relaxation of artificial irregularities was recorded under conditions of ionosphere illumination over the SURA facility and the proximity of the dusk terminator at ionospheric heights to the magnetically conjugate point. One possible explanation was the formation of a waveguide channel for electromagnetic wave propagation between conjugate regions (along a magnetic field line) due to processes in the vicinity of the terminator [Yampolskii, 1989; Nasyrov, 1991; Blagoveshchenskaya et al., 2007; Frolov et al., 2008; Hysell et al., 1996]. The recorded wave processes with periods in the range of magnetic pulsations Pc3-4 [Blagoveshchenskaya et al., 2007] indicate the presence of Alfvén waves in the magnetic flux tube, which can cause secondary instability over the SURA facility. The development of secondary instability can shed light on changes in the properties of the generated artificial turbulence and an increase in natural ionospheric irregularities with scales $l_\perp$>100 m.

The dusk terminator on October 21, 2019 at 15:00–16:00 UT was located along the geodetic line connecting Tromsø (69.6° N, 19.2° E) and the magnetically conjugate point (61.2° S, 66.7° E at altitudes from Earth's surface to 100 km in the ionosphere). The F2-layer ionosphere over Tromsø was illuminated, so we can assume that the long relaxation times of SAIIs in ADR over Tromsø during O-heating on October 21, 2019 (more than 10–20 s) can be explained by the influence of interaction processes between the ionospheric regions over Tromsø and the ionospheric region adjacent to it under conditions when they are located near the solar terminator boundaries.

2.3. February 25, 2013 experiment

The EISCAT/Heating facility on February 25, 2013 emitted in the morning at a frequency f_H=5.423 MHz of ordinary (O-mode) polarization toward the magnetic zenith in the mode of 10 min heating — 5 min pause. Phased array antenna No. 1 with beamwidth of ~5–7° was employed. The effective power of the facility P_{eff}~450 MW. The horizontal size of ADR in the F2 layer in the threshold power of the heating facility's HF radio wave was ~ 75 km. The experiment was conducted during low solar and quiet magnetic activity (W=25, K_p=1). SAII excitations in the ionosphere over Tromsø were observed from 08:30 to 09:15 UT (LT=UT+2 hrs) by the method of bistatic scattering along the diagnostic paths Irkutsk—Tromsø—St. Petersburg, f_{diagn}=21.8 MHz, and Moscow—Tromsø—Lovozero, f_{diagn}=12.075 MHz (the map in Figure 1). In the experiment, we used diagnostic radio paths with various receivers and transmitters. Both paths are fully illuminated. Values of f_oF2 over the heating facility during this period were 5.7–6.0 MHz, $f_H < f_o$F2; therefore, SAIIs can be generated in the ionosphere during cycles of emission of a powerful HF radio wave.

Figure 4 presents sonograms measured by the Doppler method along two diagnostic paths on February 25, 2013 from 08:30 to 09:15 UT (Figure 4, *a*, *b*). Along the time axis are emission cycles of the facility's transmitter. Minimum transverse dimensions $l_\perp$ of scattering SAIIs are given for the conditions of measurements

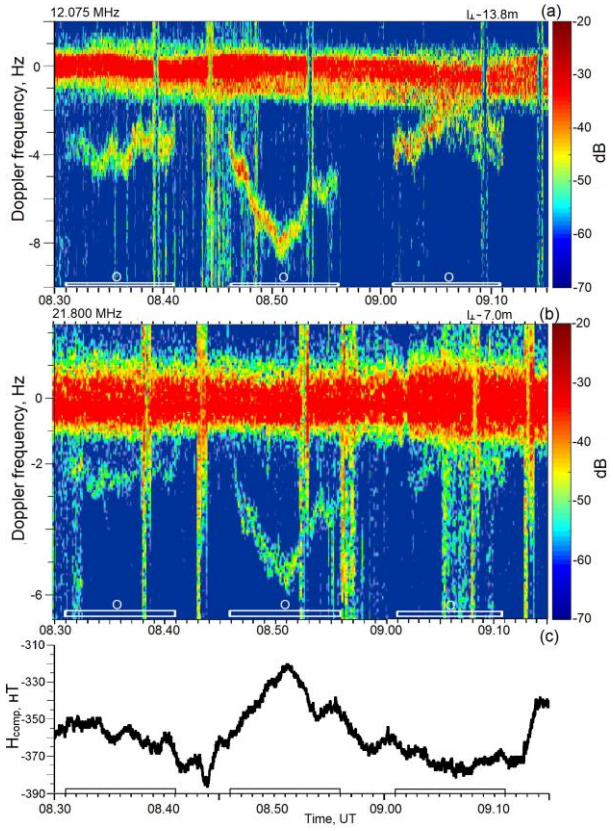

Figure 4. Sonograms obtained along the diagnostic paths Irkutsk—Tromsø—St. Petersburg, f_{diagn}=21.8 MHz, on February 25, 2013 at 08:30–09:15 UT (*a*); Moscow—Tromsø—Lovozero, f_{diagn}=12.075 MHz (*b*); the geomagnetic field H component of the magnetovariation station Tromsø (*c*)

carried out along the paths Irkutsk—Tromsø—St. Petersburg, f_{diagn}=21.8 MHz ($l_\perp$~7 m), and Moscow—Tromsø—Lovozero, f_{diagn}=12.075 MHz ($l_\perp$~13.8 m).

During operation of the EISCAT/Heating facility, bistatic scattered signals at frequencies f_D shifted toward the negative direction from f_D=0 corresponding to the direct signal of propagation over the transmitter—receiver path were recorded in the negative part of the Doppler spectrum. Note the large number of external interference recorded during measurements, which were caused by the operation of transmitters of vertical and oblique chirp sounding stations located on the territories of the receiving stations Gorkovskaya and Lovozero. Transmitting and receiving antennas of the complexes on the territories of the stations are placed in close proximity to the multichannel Doppler equipment. In sonograms, bistatic scattered signals featured a 1.3–1.5 Hz Doppler spectrum width and ~3–4 and 17 min wave variations in f_D. There is a correlation between $f_D(t)$ variations along both diagnostic paths, which coincided with the periods of oscillations of the magnetic field H component (Figure 4, *c*), measured by the magnetovariation station Tromsø [https://flux.phys.uit.no/ArcMag/].

3. Modeling

3.1. Trajectory characteristics

To analyze the measurements by the HF radio channel model [Borisova et al., 2002], we have calculated ray trajectories of propagation of diagnostic HF signals along transmitter—ADR paths over Tromsø—receiver, taking into account bistatic scattering by small-scale field-aligned irregularities in the ionosphere over the EISCAT/Heating facility. The HF radio channel model is designed to solve the wave equation and calculate signal propagation trajectories in an anisotropic inhomogeneous and nonstationary medium. Integration along the radio signal propagation beam is carried out by the geometrical optics method, taking into account smooth horizontal irregularities of the ionosphere, in the framework of the two-scale expansion approximation. Spatial and temporal variations in the electron density of the ionosphere N_e along the radio wave propagation path are described by the global ionosphere model based on the combination of known global models of ionospheric layers E, F1, F2 and interlayer valleys describing regular dependences of N_e variations on latitude, longitude, altitude, time of day, day of the year, solar and magnetic activity, given by the Wolf number W and the three-hour index K_p [Chernyshev, Vasilyeva, 1975; Anufrieva, Shapiro, 1976; Rawer et al., 1978]. The model also accounts for the features of the high-latitude ionosphere: the main ionospheric trough and sporadic ionization in the E and F layers [Blagoveshchenskii, Zherebtsov, 1987]. Input parameters of the model are W, K_p, time of day t, day of the year, geographic coordinates of diagnostic signal transmitter and receiver, diagnostic signal frequency f_{diagn}, geographic coordinates of the HF heating facility, pump frequency f_H. Electron density distributions with height $N_e(h)$ are represented by a set of nine quasi-parabola segments with continu-

ous values at junctions of both the functions $N_e(h)$ themselves and its first derivatives $dN_e(h)/dh$. The introduced quasi-parabolic approximation of the $N_e(h)$ profile allows for exact integration of the eikonal equation. When modeled at a given integration step, the ionospheric parameters are considered constant. The integration step in the longitudinal direction along the great-circle arc is 10–100 km and 5–30 km in height in the ionosphere. When reflecting from Earth, the effect on the reflection coefficient of the underlying land — sea surface is examined.

At each integration step, the following radio wave characteristics are calculated: ray trajectories (beam coordinates, mode, vertical and azimuthal angles, etc.), group and phase paths, Doppler frequency variations, and wave vector components.

Calculation of propagation characteristics along the research bistatic scatter paths transmitter—ADR—receiver involves searching for solutions to two propagation problems: transmitter—ADR and ADR—receiver. In the ionosphere at altitudes of ADR location over a heating facility (in this work, EISCAT/Heating), incident waves of diagnostic signals are bistatically scattered by SAIIs and further propagate to a receiver. The boundary condition for connecting the solutions of the two propagation problems is to fulfill the conditions for the formation of a cone of specular scattering by incident and scattered waves, for which the relation is valid [Gershman et al., 1984]

$$\mathbf{k}_0 \cdot \mathbf{H} = \mathbf{k}_s \cdot \mathbf{H}, \quad (2)$$

where $\mathbf{k}_0$ and $\mathbf{k}_s$ are the wave vectors of incident and scattered waves respectively; **H** is the geomagnetic field vector. The trajectories that implement the reception of diagnostic HF radio signals in a receiver are found by sorting through radiation angles. The results of 3D modeling of radio signal propagation trajectory along the transmitter—ADR — receiver path in Figures 5, 6 are shown in a single coordinate plane range — height with the junction in the ADR location range. These figures display isolines of ionospheric plasma frequencies along radio paths.

The trajectory characteristics of HF radio signals were calculated for heliogeophysical conditions that took place during the heating experiments. Examples of modeling propagation trajectories of diagnostic signals from transmitters, located in North America, for geophysical conditions on October 21, 2019 (W=0, K_p=1, t=15.20 UT) are given in Figure 5. With the distribution of natural ionospheric gradients along radio paths, diagnostic HF radio signals can propagate from a transmitter to ADR along a multi-hop trajectory with reflection from the F2 layer. For the Nashville transmitter at f_{diagn}=15.825 MHz, propagation to ADR is realized by 3F2 modes with reflection from the F2 layer and 3F2 modes with "deflection" (without intermediate reflection from Earth's surface). For the Hialeah Gardens transmitter (15.770 MHz) there may be 3F2 modes with deflection and 4F2 hop modes. For the Nashville signal with f_{diagn}=13.845 MHz, propagation to ADR is possible with 3-4F2 modes, a waveguide mechanism in the E–F channel, and deflection modes with reflection from the F2 layer. After bistatic scattering by ionospheric irregularities to a receiver (St. Petersburg), signals propagate without intermediate reflection.

Vertical angles of diagnostic signal wave vector $\mathbf{k}_0$ directions calculated in ADR on October 21, 2019 varied from 80° to 90° (from vertical). Under conditions of regular dusk gradients of F2-layer electron density distribution along radio paths, there may be propagation trajectories of HF signals from the Nashville and Hialeah Gardens transmitters with deflection. This type of propagation provides a higher level of wave field incident on ADR and hence a higher level of P_{SAII} of bistatic scattered signals. Simultaneous scattering of several (two or three) modes over long radio paths with close directions of incident wave vectors $\mathbf{k}_0$ onto ADR leads to an increase in the spread of f_D and to the inability to identify tracks of individual modes in sonograms. In the case of separating the angles of incidence of wave vectors of individual propagation modes, several f_D tracks corresponding to different propagation modes and recorded by the bistatic scattering method are observed in sonograms, for example, along paths shorter than 3000 km (e.g., [Belenov et al., 1977; Borisova et al., 2007, 2009; Blagoveshchenskaya et al., 2006]). In this experiment, vertical angles of incidence $\mathbf{k}_0$ of various multi-hop trajectories onto ADR were close to ~80°–90° and did not allow us to identify individual "tracks" of bistatic scattered signals and the component of vertical motion of irregularities along the magnetic field.

A decrease in the power of direct signals P_{DS} and at outshifted frequencies of P_{SAII} for transmitters from America on October 21, 2019 with frequencies f_{diagn}=15.825 MHz after 15:33 UT (see Figure 3, *a*) and f_{diagn}=15.770 MHz after 15:37 UT (see Figure 3, *b*) is explained by model data. To fulfill the condition for the formation of a specular scattering cone over Tromsø for an incident radio wave and scattered in the direction of St. Petersburg during the rise of the F2-layer peak height for signals at frequencies above 15.5 MHz, the reflection height from the F2 layer should be increased. Consequently, propagation paths of HF radio waves change (in this experiment along a path of given length, trajectories with deflection disappear and appear with a larger number of jumps, which leads to a decrease in the signal level). At the same time, the propagation mechanism at 13.845 MHz remains unchanged until 16 UT.

Results of the trajectory modeling for experimental conditions on February 25, 2013 are presented in Figure 6. Despite the difference between lengths of the bistatic scatter radio paths (2470 and 5660 km) and the values of diagnostic frequencies, propagation of radio signals from Moscow to Lovozero, f_{diagn}=12.075 MHz, and from Irkutsk to St. Petersburg, f_{diagn}= 21.8 MHz is implemented by the same 2F2 trajectory modes. Figure 6 demonstrates the possibility of receiving bistatic scattered signals with hop trajectories propagating to ADR over Tromsø and then, after bistatic scattering, to the receiver. With the distribution of F2-layer natural gradients along radio paths during the day, the range of heights in which diagnostic HF radio signals fall on ionospheric irregularities over Tromsø was 200–220 km in the F layer. The vertical angles of the diagnostic signal wave vector $\mathbf{k}_0$ orientation in ADR for trajectories realizing the reception of bistatic scattered signals by receivers varied from 85° to 90°.

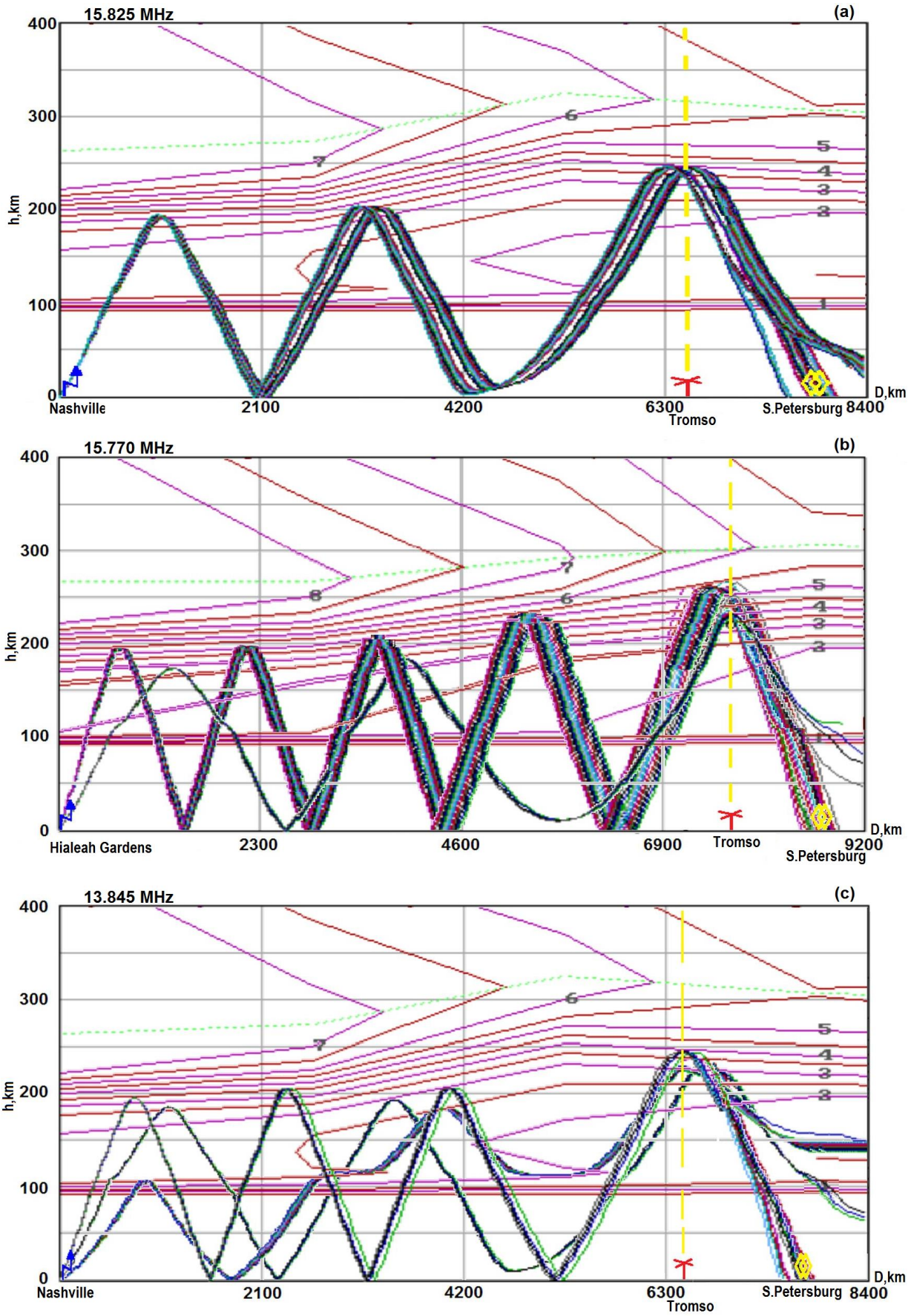

Figure 5. Propagation paths of diagnostic HF signals during the heating experiment on October 21, 2019: the Nashville—Tromsø—St. Petersburg path, f_{diagn}=15.825 MHz (*a*) and f_{diagn}=13.845 MHz (*c*); the Hialeah Gardens—Tromsø—St. Petersburg path, f_{diagn}=15.77 MHz (*b*);

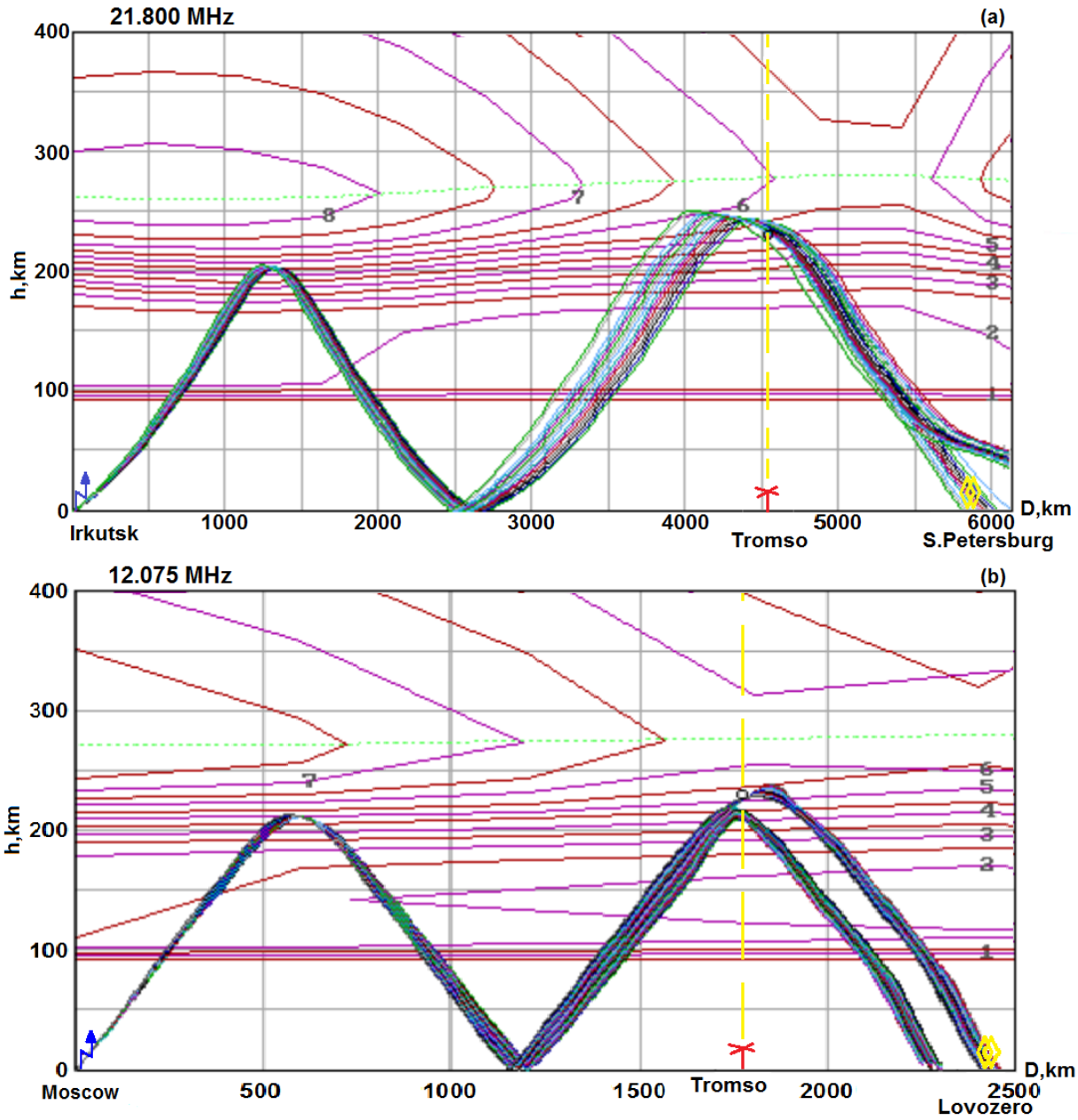

Figure 6. Propagation trajectories of diagnostic signals on February 25, 2013 at 08.30 UT. ADR is formed at heights of the F layer in the region of reflection of a powerful pump wave (f_H=5.423 MHz)

The simulated results have shown that the available geometry of the experimental radio paths in October 2019 and February 2013 ensures stable reception of bistatic scattered signals if artificial irregularities develop at F-layer heights.

3.2. Motion of ionospheric irregularities in ADR

When calculating the SAII velocity vector, it is assumed that the scattering region is uniform for various diagnostic radio signals.

The projection of the SAII velocity **V** onto the direction of the vector $\Delta\mathbf{k}$ of difference between wave vectors of incident $\mathbf{k}_0$ and scattered $\mathbf{k}_s$ waves $\Delta\mathbf{k}=\mathbf{k}_s-\mathbf{k}_0$ is determined from the expression [Gershman et al., 1984]

$$V_{\Delta k} = \frac{f_D}{f_{diagn}} \frac{c}{2\sin(\theta/2)}, \quad (3)$$

where f_D is the Doppler frequency shift; f_{diagn} is the diagnostic radio wave frequency, c is the speed of light; θ is the bistatic scattering angle; γ_0 and γ_s are vertical angles; Az_{k0}, Az_{ks} are azimuths of $\mathbf{k}_0$ and $\mathbf{k}_s$; for the scattering angle the expression is valid

$$\cos\theta = \cos\gamma_0 \cos\gamma_s \cos(Az_{k0} - Az_{ks}) + \\ + \sin\gamma_0 \sin\gamma_s. \quad (4)$$

From bistatic measurements of Doppler frequency shifts f_D, two projections of the velocity of irregularities V_{k1} and V_{k2} are calculated along two diagnostic radio paths. From $V_{\Delta k1}$ and $V_{\Delta k2}$, the amplitude V and the azimuthal direction Az_V of the velocity vector of ionospheric irregularities **V** are determined provided that

ADR dimensions are neglected [Blagoveshchenskaya et al., 2006; Borisova et al., 2007]

$$V = V_{\Delta k2} / \cos\left\{\text{arctg}\left[\left(\cos\alpha - \beta\right)/\sin\alpha\right]\right\},$$
$$Az_V = Az_{k1} - \text{arctg}\left[\left(\cos\alpha - \beta\right)/\sin\alpha\right], \quad (5)$$

where V_{k1}/V_{k2}, $\alpha = Az_{k1} - Az_{k2}$ are the angles between azimuthal directions of $\Delta\mathbf{k}_1$ and $\Delta\mathbf{k}_2$ (Az_{k1} and Az_{k2}) along the first and second diagnostic paths respectively.

3.2.1. Numerically estimated effect of the radio signal scattering angle and the azimuth of motion of ionospheric irregularities in ADR on calculation of velocity amplitude

The parameters α and β in (5) are found from experimental measurements of f_D and from calculations of azimuthal directions of the wave vectors $\mathbf{k}_0$, $\mathbf{k}_s$, and $\Delta\mathbf{k}$ (Az_{k0}, Az_{ks}, θ, Az_{k1}, and Az_{k2}) at the bistatic scattering height. The value of the parameter β depends on the experimental values of the Doppler frequency shift f_D and the scattering angle θ. Assume that the observed value of f_D is determined only by the effect of moving irregularities in ADR.

Figure 7 illustrates changes in the projection of the irregularity velocity onto the difference vector in percent $dV_{\Delta k}(\Delta\theta)$ depending on the deviation of the real θ_{real} and calculated θ_{calc} scattering angles $\Delta\theta = \theta_{real} - \theta_{calc}$ for the diagnostic paths of interest (see Table 1). For $\theta > 0.5°$, $dV_{\Delta k}(\Delta\theta)$ are close to linear approximations. Deviations of the scattering angle by 1°–5° for transmitters located in America cause significant errors in defining $V_{\Delta k}$ and hence α and β. The error in determining $V_{\Delta k}$ decreases sharply to 3 % if the deviations $\Delta\theta < 0.3°$.

The azimuth angle of propagation of a radio wave bistatically scattered by ionospheric irregularities toward St. Petersburg $Az_{ks} \sim 147°$ (or 98° in Lovozero). Its value can vary from 145° to 150° in view of ADR's horizontal dimensions ~55 km when using PAA-2 on October 21, 2019. In the February 25, 2013 experiment, when the facility transmitted to PAA-1, Az_{ks} in the direction of St. Petersburg varies from 146° to 148°; and in the direction of Lovozero, from 97° to 99°. At a distance of 1150 km (670 km to Lovozero), these variations can be ignored and for a bistatic scattered signal the azimuth of propagation Az_{ks} to the receiver can be considered constant.

Ionospheric irregularities in N_e over a long path of diagnostic signal propagation can lead to significant deviations of radio wave Az_{k0} in the vicinity of ADR from the great-circle arc. The calculated values of the scattering angles θ and the error in Az_{k0} of wave vectors for bistatic scattered radio waves under conditions of the experiments in 2019 and 2013 are listed in Table 2. In view of (4), taking into account that in the experiments the vertical angles γ_0 and γ_s are smaller than 10°, we find that errors in calculating the scattering angle θ are determined by the error in estimating the azimuth of a diagnostic wave incident on ADR $\Delta\theta \sim \Delta Az_{k0}$. Thus, changes in the scattering angle primarily result from

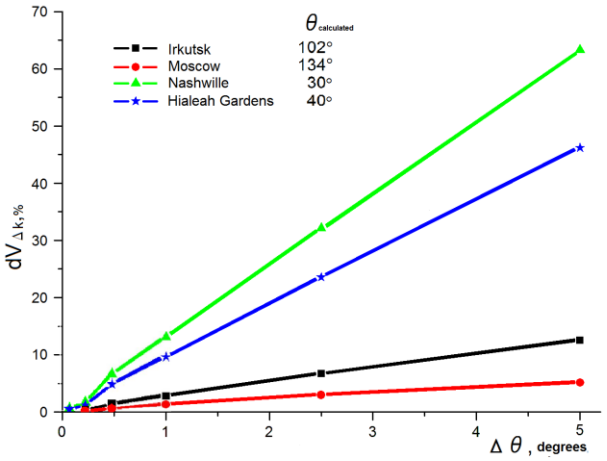

Figure 7. Variation in the SAII velocity projection onto the difference vector of scattering $dV_{\Delta k}(\Delta\theta)$ as function of deviation of the real scattering angle θ_{real} from the calculated one θ_{calc}, $\Delta\theta = \theta_{real} - \theta_{calc}$ for diagnostic bistatic scattering paths with different scattering angles θ

variations in the azimuth Az_{k0} of a wave incident on ADR.

Blagoveshchenskaya et al. [1991], using experimental measurements of diagnostic HF radio signals from transmitters located in North America (paths longer than 6000 km) in St. Petersburg, have examined the patterns of azimuth deviations from the great-circle arc. The diagnostic HF radio signals were received in the evening in winter. The research results have shown that the azimuth deviations ~5°–10° are observed under quiet geomagnetic conditions. Under conditions of moderate disturbance, the deviations may be as large as 20°–30°.

For a specific location of the heating facility and the receiver, the azimuth angle Az_{ks} of $\mathbf{k}_s$ has been found. The angles γ_0, γ_s, Az_{k0}, Az_{ks} are related by equation of bistatic scattering cone (2). The bistatic scattering angle θ is calculated according to (4). The results indicate that under quiet geomagnetic conditions deviations of ΔAz_{k0} by 5°–10° will cause the angle $\theta \sim \pm 0.25°$ to change. Taking into account the data presented in Figure 7, the error in calculating the SAII velocity modulus (assuming $\Delta Az_{k0} \sim 5°–10°$) from Doppler measurements of transmitters from North America will be smaller than 2–3 %.

Thus, in October 2019 from 15:20 to 15:48 UT (under quiet geomagnetic conditions), calculations of the amplitude of $|\mathbf{V}|$ from (5) depend largely on the accuracy of f_D measurement. The error in determining the Doppler frequency shift $\Delta f_D \sim 1.5 \div 2.5$ Hz for the observed values of $f_D \sim 2 \div 4$ Hz can cause errors in calculating the projection of the SAII velocity $|\mathbf{V}|$ onto the difference vector $V_{\Delta k} \sim 40 \div 100$ %.

The greatest changes in the parameter β occur if the SAII motion is directed perpendicular to one of the difference vectors $\Delta\mathbf{k}$ (i.e. $f_D \sim 0$) or if the diagnostic frequencies f_{diagn1} and f_{diagn2} are close. In this case, the azimuth of SAII motion Az_V can confidently be calculated with minimum reliability of the calculation of the V amplitude.

The value of the parameter α depends on the accuracy in determining the scattering angles θ_1 and θ_2. The error

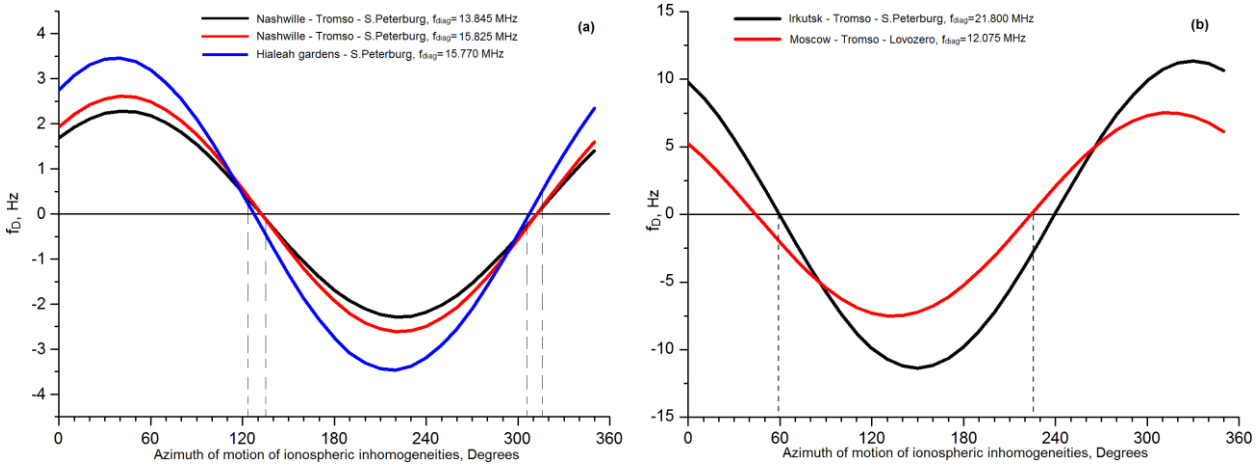

Figure 8. Calculated Doppler frequency shifts f_D depending on the azimuth of motion of irregularities in ADR over Tromsø along diagnostic paths for experiments on October 21, 2019 (*a*) and February 25, 2013 (*b*). The velocity of ionospheric irregularities $|V|$=100 m/s

in calculating the velocity of irregularities **V** increases sharply for bistatic scattering paths if measurements are performed along diagnostic radio paths with close scattering angles $\theta_1 \sim \theta_2$ and hence $\alpha \sim 0$.

To explain the effect of the SAII motion azimuth Az_V on the change in the Doppler frequency shift f_D of diagnostic HF radio signals along bistatic scattering paths, Figure 8 presents data from model calculations $f_D=f_D(Az_V)$. For the diagnostic HF radio paths of observations in the October 21, 2019 experiment Nashville—Tromsø—St. Petersburg, f_{diagn}=13.845 MHz, 15.825 MHz, and Hialeah Gardens—Tromsø—St. Petersburg, f_{diagn}=15.77 MHz, the dependences $f_D(Az_V)$ are shown in Figure 8, *a*. For the Irkutsk—Tromsø—St. Petersburg path, f_{diagn}= 21.8 MHz, and Moscow—Tromsø—Lovozero, f_{diagn}=12.075 MHz, measurements of $f_D(Az_V)$ in the February 25, 2013 experiment are illustrated in Figure 8, *b*. The dependence $f_D(Az_V)$ was calculated under the condition of constant amplitude of the velocity of ionospheric irregularities V=100 m/s. A changing in $|V|$ leads to a proportional change in f_D The data in Figure 8 shows the conditions when along the bistatic scattering paths in the 2013 and 2019 experiments shifts in f_D of the same or different signs depending on the motion direction of irregularities in the vicinity of ADR can be observed. For example, for radio signals from the Hialeah Gardens and Nashville transmitters, a negative shift in f_D is simultaneously observed when SAIIs move in the azimuth sector 135°–305°. A negative shift in f_D along the Irkutsk—Tromsø—St. Petersburg and Moscow—Tromsø—Lovozero paths is simultaneously recorded if SAIIs move in the azimuth sector 60°–225°.

3.2.2 Determining the velocity vector of ionospheric irregularities in ADR from observational results

To calculate the SAII velocity vector **V** from (3) and (5), the Doppler frequency shifts f_D of diagnostic signals at a 30 s interval are preliminarily identified in experimental data by the highest value of the spectral power distribution P_{SAII} (f_D), which formed the tracks $f_D(t)$ in sonograms.

Figure 9, *a* presents median values of $f_D(t)$ for sonograms (see Figure 3, *a*–*c*) of the radio signals from transmitters of Hialeah Gardens, f_{diagn}=15.77 MHz, and Nashville, f_{diagn}=15.825, 13.845 MHz, measured on October 21, 2019. Calculations of V for the period 15:20–15:50 UT were carried out from measurements of f_D along the paths Hialeah Gardens, f_{diagn}=15.77 MHz, and Nashville, f_{diagn}=13.845 MHz — the first pair of f_{diagn}=15.770 MHz, f_{diagn}=13.845 MHz; along the paths Hialeah Gardens, f_{diagn}=15.77 MHz, and Nashville, f_{diagon}=15.825 — the second pair of f_{diagn}=15.77 MHz, f_{diagn}=15.825 MHz (Figure 9, *b*1, *b*2).

The data presented in Figure 9, *b*1, *b*2 demonstrates a good correspondence between the azimuthal directions Az_V of SAII motion, which were calculated from f_D observations along two pairs of diagnostic bistatic scattering paths. The mean values of the SAII motion direction Az_V were similar: for the first pair $Az_V \sim (218\pm1)°$ and for the second pair $Az_V \sim (217\pm6)°$.

The mean values of the SAII velocity amplitude $|\mathbf{V}|$ and deviation $\Delta|\mathbf{V}|$ for six heating cycles on October 21, 2019 $Az_V \sim 175\pm100$, 150 ± 70, 140 ± 50, 130 ± 50, 150 ± 40, and 130 ± 50 m/s. Figure 9, *c* for two pairs of calculations shows estimated SAII moduli $|\mathbf{V}|$ and deviations $\Delta|\mathbf{V}| \sim 50 \div 100$ m/s.

According to observations along the three paths (see Figure 9), wave oscillations of $f_D(t)$ with $\tau \sim 2 \div 3 \div 14$ min were recorded, some of which were less than or equal to the heating cycle period; the oscillation range was ~1.5–2.5 Hz and was close to the spectral width of the outshifted Doppler frequencies $\Delta f_D \sim 1.5 \div 2.5$ Hz. In a similar variation in $f_D(t)$, errors in determining simultaneous values of f_D along different diagnostic radio paths can cause large errors. SAII V in the presence of wave variations in $f_D(t)$ was also calculated using pre-averaged f_D for a 180 s heating cycle. The SAII motion directions Az_V for both pairs of calculations in this variant were $(217\pm1)°$ and coincided with the results of 217° and 218° obtained from 30 s averaging data. The results of calculations of $|\mathbf{V}|_{SAII}$ are presented in Figure 9, *c* (with crossed-out triangles for 180 s averaging). The data

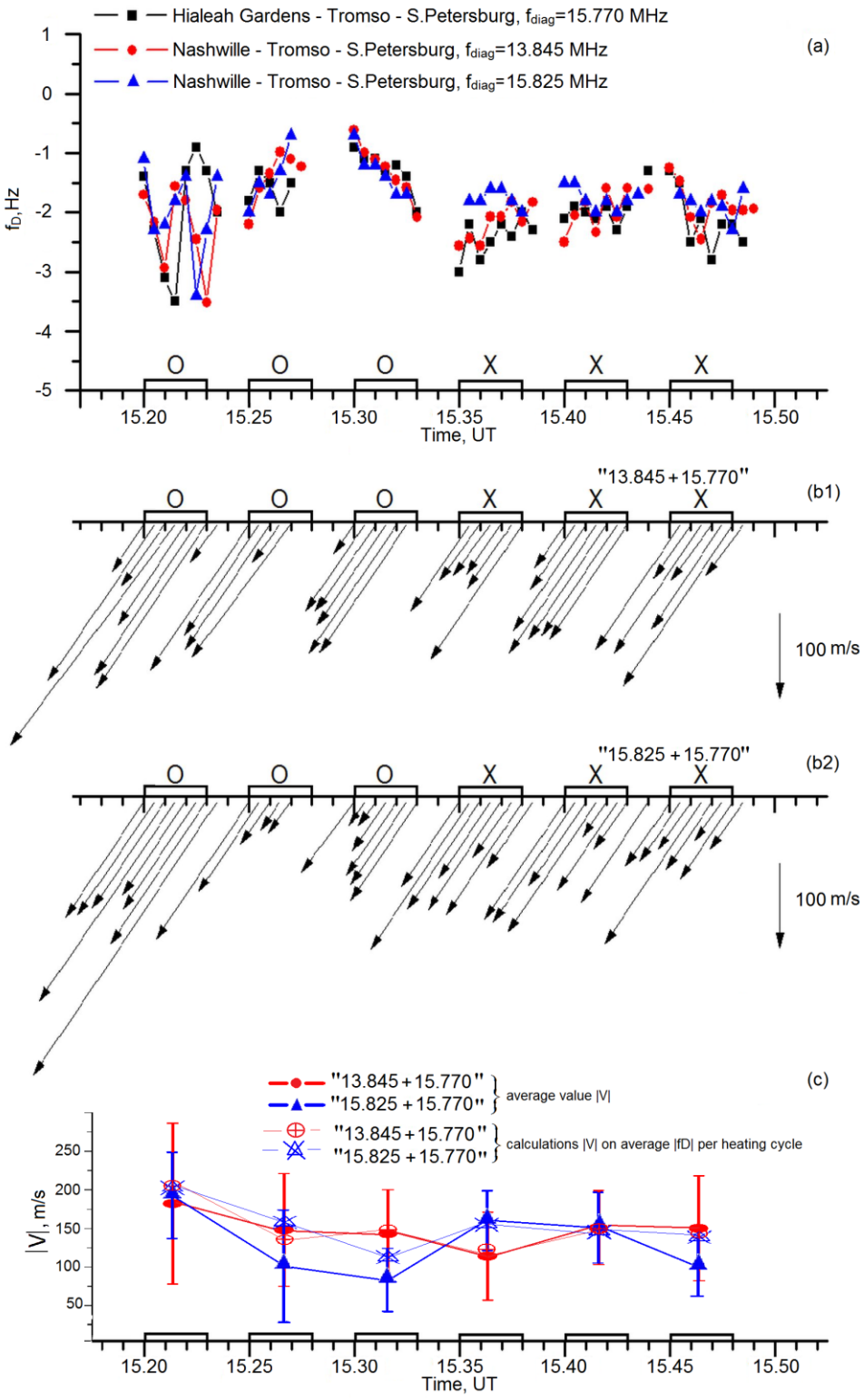

Figure 9. Median values of f_D of diagnostic HF signals scattered by ADR irregularities on October 21, 2019 along paths for North American transmitters (*a*); SAII velocity vectors calculated from Doppler measurements along the paths Hialeah Gardens—Tromsø—St. Petersburg, f_{diagn}=15770 kHz, and Nashville—Tromsø—St. Petersburg, f_{diagn}=13845 kHz (*b1*); Hialeah Gardens—Tromsø—St. Petersburg and Nashville—Tromsø—St. Petersburg, f_{diagn}=15825 kHz (*b*2); average |**V**| and calculations of |**V**| from average $|f_D|$ per heating cycle (*c*). The emission periods of the HF heating facility are indicated on the time axis

(Figure 9, *c*) suggests that there is agreement between the average values of *V* calculated from the data on f_D, averaged over 30 or 180 s intervals. With wave variations in $f_D(t)$ with periods close to the intervals of heating cycles, |**V**| of SAII motion can be estimated from average f_D per cycle.

For the February 25, 2013 experiment, Figure 10, *a* presents median values of f_D at a 30 s interval, diagnostic HF signals along the paths Irkutsk—Tromsø—St. Petersburg, f_{diagn}=21.8 MHz, and Moscow—Tromsø—Lovozero, f_{diagn}=12.075 MHz. Figure 10, *b* presents the results of calculation of the SAII velocity vector **V** from Doppler measurements along two diagnostic radio paths on February 25, 2013. Averages of the SAII velocity modulus |**V**| and deviation Δ|**V**| for three heating cycles on February 25, 2013 are shown in Figure 10, *c*. Periods of EISCAT/Heating emission are indicated on the time axis.

According to the calculation results, SAIIs moved in the azimuthal direction (184±7). For February 25, 2013, Figure 10, *c* displays averages of velocity |**V**| and deviation Δ|**V**| for each heating cycle, which were 70±20, 110±30, 50±15 m/s respectively. Averages of the azimuthal direction Az_V in three cycles Az_V~225°, 228°, and 230°.

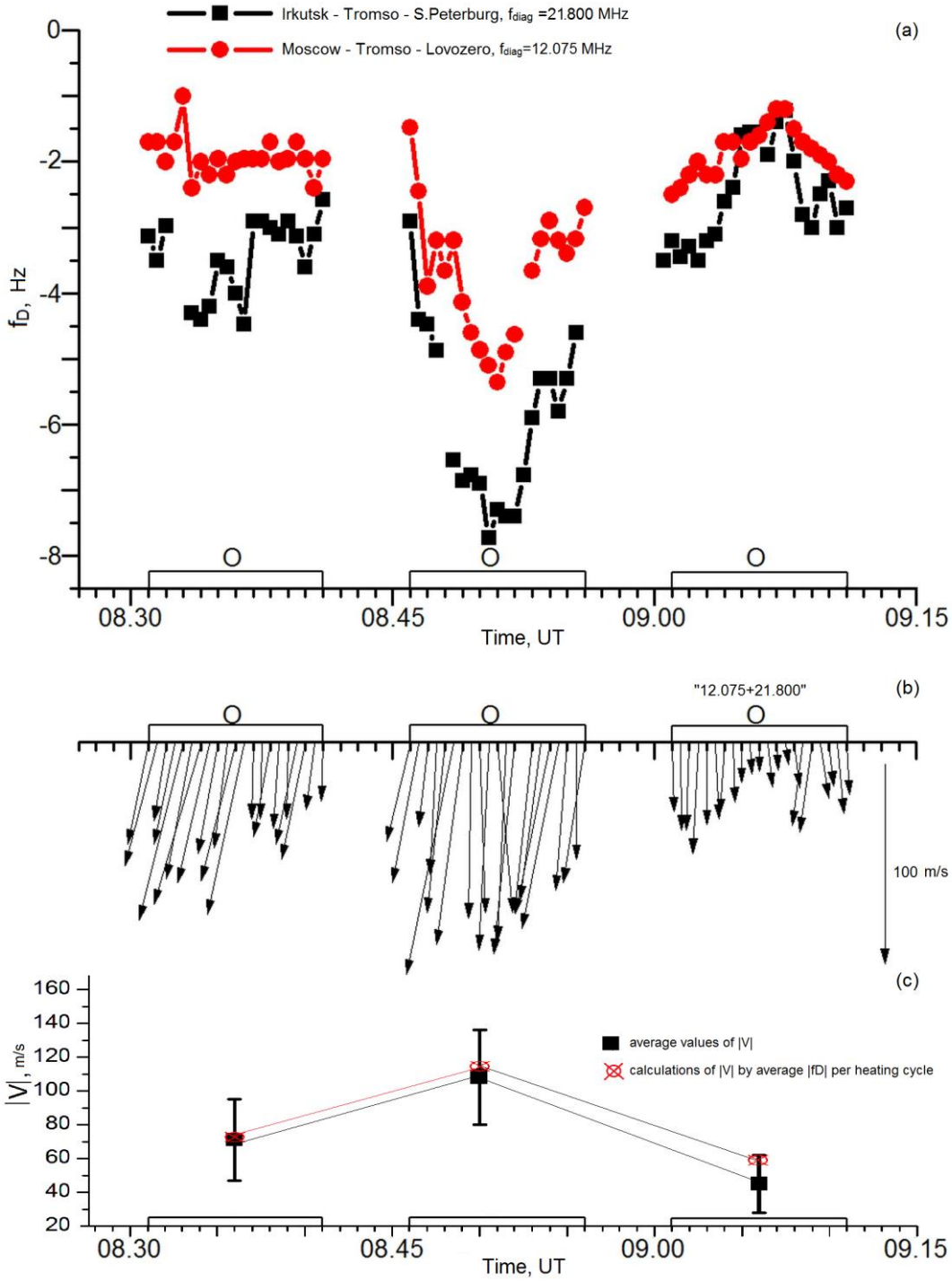

Figure 10. Median values of the Doppler frequency shift f_D of diagnostic HF signals in the February 25, 2013 experiment (*a*); SAII velocity vectors calculated from Doppler measurements along the paths Irkutsk—Tromsø—St. Petersburg and Moscow—Tromsø—Lovozero (*b*); average |**V**| and calculations of |**V**| from average $|f_D|$ per heating cycle (*c*). Periods of HF heating facility emission are indicated on the time axis

On February 25, 2013, Doppler scattered signals had wave variations in $f_D(t)$ with 3–4–17 min periods and an oscillation range f_D~1.5÷5.0 Hz. The spectral width of the signals was Δf_D~1.0÷2 Hz. Calculations of $|\mathbf{V}|_{SAII}$ averaged per cycle are shown in Figure 10, *c* for f_D averaged over 30 s and over a 600 s heating cycle. The values of Az_V according to f_D, averaged over the 600 s heating cycle, in three cycles were Az_V~223°, 226°, and 230°.

Averages of $|V|_{SAII}$ were 100–200 m/s in the evening on October 21, 2019 and $|V|_{SAII}$~50÷110 m/s in the morning on February 25, 2013. The calculated values of $|V|_{SAII}$ are within the range of irregularity drift velocities 5–380 m/s, observed, for example, in [Borisova et al., 2007; Sivokon, 2020; Eglitis et al., 1998; Blagoveshchenskaya et al., 2006; Yampolskii et al., 2019].

DISCUSSION AND CONCLUSION

During the 2013, 2016, and 2019 experiments, the high-latitude ionosphere was modified by powerful HF radio waves of ordinary or extraordinary polarization emitted by the EISCAT/Heating facility (Tromsø, Norway).

In experiments with the EISCAT/Heating facility on October 20, 2016, the SAII behavior was simultaneously observed by the CUTLASS HF radar and Doppler measurements over radio paths 6000–9000 km long. Comparing the characteristics of SAIIs, simultaneously measured during X-heating by the CUTLASS HF radar and by the method of bistatic scattering of diagnostic HF radio signals over long radio paths (see Table 3) has shown similar parameters of SAII development (rise and relaxation times, P_{SAII}, behavior of P_{SAII} over time) depending on the relations between f_H, f_oF2, and f_xF2.

The frequency range of the CUTLASS HF radar emission is 8–20 MHz; therefore, radio signals are backscattered by SAIIs with minimum transverse scales $l_\perp$ from 7.5 to 19 m. Doppler observations of 14–18 MHz diagnostic frequencies over long bistatic scattering paths of the North America—Tromsø—St. Petersburg transmitter from azimuthal directions 280°–305° expand the range of detection of SAIIs with transverse scales $l_\perp$ to 19–28 m (8–11 m during backscattering).

In sonograms measured in 2013, 2016, and 2019, bistatic scattered signals exhibited wave variations in $f_D(t)$ with ~2–4 and 14–17 min periods coinciding with the periods of the geomagnetic field *H*-component oscillations measured at the magnetovariation station Tromsø [https://flux.phys.uit.no/ArcMag/]. Thus, the SAII motion is modulated by field line oscillations in the ionosphere over Tromsø. To estimate the SAII velocities *V* over the cycle period in the presence of wave variations in $f_D(t)$, it is sufficient to calculate them from previously estimated average f_D for each cycle.

The results of modeling of trajectory characteristics of diagnostic HF radio signal propagation over long paths, obtained by the ionospheric HF radio channel model, have shown that in the evening of the October 2019 experiment HF radio wave trajectories took place without intermediate reflection from Earth's surface (with deflection or waveguide character). This fact significantly increases the power level of radio waves, incident on the scattering region, and bistatic scattered signals. We have determined vertical and azimuth angles of arrival of wave vectors at heights of bistatic scattering in ADR in order to calculate bistatic scattering angles.

From measurements of Doppler shifts f_D of diagnostic HF radio signals by the bistatic scattering method, SAII velocity vectors **V** in the ionosphere have been calculated simultaneously along several paths. We have analyzed possible errors in calculating the modulus *V* and azimuth Az_V of ionospheric irregularities, using the method considered.

From the model results and experimental data we have found that in the evening hours of October 21, 2019 average velocities of ionospheric irregularities varied from 100 to 200 m/s in a southwesterly direction. In the morning hours of February 25, 2013, SAIIs moved southward. The velocities $|\mathbf{V}|_{SAII}$ varied from 45 to 108 m/s.

We thank the international scientific association EISCAT. The work was financially supported by the Russian Science Foundation (Grant No. 22-17-00020), [https://rscf.ru/project/22-17-00020/].

REFERENCES

Afraimovich E.L. *Interferential methods of the ionosphere radio sounding*. Moscow, Nauka, 1982, 198 p. (In Russian).

Anufrieva T.A., Shapiro B.S. *Geometricheskie parametry sloya F2 ionosfery* [Geometric parameters of the ionospheric F2 layer]. Moscow, Nauka Publ., 1976, 91 p. (In Russian).

Avdeev V.B., Belei V.S., Belenov A.F., Galushko V.G., Erukhimov L.M., Myasnikov E.N., et al. Review of results of HF scattering by artificial ionospheric turbulence obtained with UTR-2. *Radiophysics and Quantum Electronics*. 1994, vol. 37, no. 4, pp. 299–307.

Belenov A.F., Bubnov V.A., Erukhimov L.M., Kiselev Yu.V., Komrakov G.P., Mityakova É.E., et al. Parameters of artificial small-scale ionospheric irregularities. *Radiophysics and Quantum Electronics*. 1977, vol. 20, no. 12, pp. 1240–1245.

Blagoveshchenskaya N.F. Perturbing the high-latitude upper ionosphere (F region) with powerful HF radio waves: A 25-year collaboration with EISCAT. *URSI Radio Sci. Bull*. 2020, iss. 373, pp. 40–55. DOI: 10.23919/URSIRSB.2020.9318436.

Blagoveshchenskaya N.F., Baranets A.N., Borisova T.D., Bubnov V.A. Deviation of decameter radio waves from the great circle path at high latitudes. *Radiophysics and Quantum Electronics*. 1991, vol. 34, no. 2, pp. 102–105.

Blagoveshchenskaya N.F., Borisova T.D., Kornienko V.A., Moskvin I.V., Rietveld M.T., Frolov V.L., et al. Probing of medium-scale traveling ionospheric disturbances using HF-induced scatter targets. *Ann. Geophys*. 2006, vol. 24, pp. 2333–2345.

Blagoveshchenskaya N.F., Borisova T.D., Kornienko V.A., Frolov V.L., Rietveld M.T., Brekke A. Some distinctive features in the behavior of small-scale artificial ionospheric irregularities at high and midlatitudes. *Radiophysics and Quantum Electronics*. 2007, vol. 50, no. 8, pp. 619–632.

Blagoveshchenskaya N.F., Borisova T.D., Yeoman T.K., Rietveld M., Ivanova I.M. Baddeley L.J. Artificial field-aligned irregularities in the high-latitude F region of the ionosphere induced by an X-mode HF heater wave. *Geophys. Res. Lett.* 2011, vol. 38, L08802. DOI: 10.23919/URSIGASS49373.

2020.9232263.

Blagoveshchenskaya N.F., Borisova T.D., Kalishin A,S., Kayatkin V.N., Yeoman T.K., Haggstrom I. Comparison of the effects induced by the ordinary (O-mode) and extraordinary (X-mode) polarized powerful HF radio waves of polarizations in the high-latitude ionospheric F region. *Cosmic Res.* 2018, vol. 56, no. 1, pp. 11–25. DOI: 10.1134/S0010952518010045.

Blagoveshchenskaya N.F., Borisova T.D., Kalishin A,S., Yeoman T.K., Shmelev Yu.A., Leonenko E.E. Characteristics of small-scale ionospheric irregularities in high-latutude F region induced by powerful HF radio waves of extraordinary polarization. *Geomagnetizm i aeronomiya* [Geomagnetism and Aeronomy]. 2019, vol. 59, no. 6, pp. 759–773. DOI: 10.1134/S001679401906004X. (In Russian).

Blagoveshchenskaya N., Borisova T., Kalishin A., Egorov I., Yeoman T., Haggstrom I. Simultaneous action of X- and O-Mode HF pump waves on the high-latitude upper (F-region) ionosphere at EISCAT. *Universe*. 2022, vol. 8, no. 2, pp. 91–111. DOI: 10.3390/universe 8020091.

Blagoveshchenskaya N.F., Borisova T.D., Kalishin A.S., Egorov I.M. Artificial ducts created via high-power HF radio waves at EISCAT. *Remote Sens*. 2023, vol. 15, iss. 10, p. 2300. DOI: 10.3390/rs15092300.

Blagoveshchenskii D.V., Zherebtsov G.A. *Vysokoshirotnye geofizicheskie yavleniya i prognozirovanie korotkovolnovykh radiokanalov* [High-Latitude Geophysical Phenomena and Prediction of HF Radio Channels]. Moscow, Nauka Publ., 1987, 272 p. (In Russian).

Borisova T.D., Blagoveshchenskaya N.F., Moskvin I.V., Rietveld M.T., Kosch M.J., Thidé B. Doppler shift simulation of scattered HF signals during the Tromsø HF pumping experiment on 16 February, 1996. *Ann. Geophys*. 2002, vol. 20, pp. 1479–1486. DOI: 10.5194/ angeo-20-1479-2002.

Borisova T.D., Blagoveshchenskaya N.F., Kornienko V.A., Rietveld M. Determining the ionospheric irregularity velocity vector based on Doppler measurements in the artificially modified F-2 region of the polar ionosphere. *Geomagnetism and Aeronomy*. 2007, vol. 47, no. 1, pp. 76–84. DOI: 10.1134/ S0016793207010124.

Borisova T.D., Blagoveshchenskaya N.F., Kornienko V.A., Frolov V.L., Vertogradov G.G., Vertogradov V.G. Splitting of the Doppler frequency shift of bi-static backscatter signals during the Sura experiments. *Geomagnetism and Aeronomy*. 2009, vol. 49, no. 4, pp. P. 510–518.

Borisova T.D., Blagoveshchenskaya N.F., Yeoman T.K., Haggstrom I. Excitation of artificial ionospheric turbulence in the high-latitude ionospheric F region as a function of the EISCAT/Heating effective radiated power. *Radiophysics and Quantum Electronics*. 2017, vol. 60, no. 1, pp. 273–290.

Chernyshov D.V., Vasilyeva T.N. *Prognoz Maksimalnykh Primenimykh Chastot*: *W*=10, 50, 150, 200 [Prediction of Maximal Applied Freguencies: *W*=10, 50, 150, 200]. Moscow, Nauka Publ., 1975, 54 p. (In Russian).

Dimant Ya.S. Dissipative parametric instability in strongly ionized plasma. *Radiophysics and Quantum Electronics*. 1977, vol. 20, pp. 1259–1267.

Eglitis P., Robinson T.R., Rietveld M.T., Wright D.M., Bond G.E. The phase speed of artificial field-aligned irregularities observed by CUTLASS during HF modification of auroral ionosphere. *J. Geophys. Res*. 1998, vol. 103, no. A2, pp. 2253–2259. DOI: 10.1029/ 97JA03233.

Erukhimov L.M., Metelev S.A., Mityakova E.E., Myasnikov E.N., Rakhlin A.V., Uryadov V.P., Frolov V.L. Experimental research in artificial ionospheric turbulence. *Teplovye Nelineinye Yavlenya v Plazme* [Plasma Thermal Nonlinear Phenomena]. Gorky, 1979, pp. 7–45. (In Russian).

Erukhimov L.M., Metelev S.A., Myasnikov E.N., Mityakov N.A., Frolov V.L. Artificial ionospheric turbulence (Review). *Radiophysics and Quantum Electronics*. 1987, vol. 30, no. 2, pp. 156–171.

Fejer J.A. Ionospheric Modification and Parametric Instabilities. *Rev. Geophys. Space Phys*. 1979, vol. 17, no. 1, pp. 135–154. DOI: 10.1029/RG017i001p00135.

Frolov V.L. *Iskusstvennaya Turbulentnost Sredneshirotnoi Ionosfery* [Artificial Turbulence in Midlatitude Ionosphere]. Nizhni Novgorod, State University Publ., 2017, 468 p. DOI: 10.31857/S0023420622040045. (In Russian).

Frolov V.L., Erukhimov L.M., Metelev S.A., Sergeev E.N. Temporal behaviour of artificial small-scale ionospheric irregularities: Review of experimental results. *J. Atmos. Solar-Terr. Phys.* 1997, vol. 59, no. 18, pp. 2317–2333. DOI: 10.1016/S1364-6826(96)00126-5.

Frolov V.L., Vertogradov G.G., Vertogradov V.G. On specific features of diurnal variations in characteristics of the diagnostic stimulated electromagnetic emission and their relation to the evolution of artificial ionospheric irregularities. *Radiophysics and Quantum Electronics*. 2008, vol. 51, no. 4, pp. 247–258.

Frolov V.L., Bolotin I.A., Komrakov G.P., Vertogradov G.G., Vertogradov V.G., Vertogradova E.G. Gyroharmonic features of the HF-induced ionospheric irregularities. *Radiophysics and Quantum Electronics*. 2012, vol. 55, no. 12, pp. 357–381. DOI: 10.1007/s11141-012-9374-0.

Gershman B.N., Erukhimov L.M., Yashin Yu. Ya. *Volnovye Yavleniya v Ionosfere i Kosmicheskoi Plazme* [Wave Phenomena in the Ionosphere and in the Cosmic Plasma]. Moscow, Nauka Publ., 1984, 392 p. (In Russian).

Grach S.M., Trakhtengerts V.Yu. Parametric excitation of ionospheric irregularities extended along the magnetic field. *Radiophysics and Quantum Electronics*. 1975, vol. 18, no. 9, pp. 951–957. DOI: 10.1007/BF01038190.

Grach S.M., Karashtin A.N., Mityakov N.A., Rapoport V.O., Trakhtengerts V.Yu. Parametric interaction between electro-magnetic radiation and ionospheric plasma. *Radiophysics and Quantum Electronics*. 1977, vol. 20, no. 12, pp. 1254–1258.

Grach S.M., Sergeev E.N., Mishin E.V., Shindin A.V. Dynamic properties of ionospheric plasma turbulence driven by high-power high-frequency radio waves. *Physics-Uspekhi*. 2016, vol. 186, no. 11, pp. 1091–1128. DOI: 10.3367/UFNe.2016. 07.037868.

Greenwald R.A., Baker K.B., Dudeney J.R., Pinnock M., Jones T.B., Thomas E.C. DARN/SuperDARN: A global view of the dynamics of high-latitude convection. *Space Sci.: Space Sci. Rev*. 1995. Vol. 71. P. 761–796. DOI: 10.1007/BF00751350.

Gurevich A.V. Nonlinear phenomena in the ionosphere. *Physics-Uspekhi*. 2007, vol. 50, no. 11, pp. 1091–1121. DOI: 10.1070/PU2007v050n11ABEH006212.

Hysell D.L., Kelley M.C., Yampolski Y.M., Beley V.S., Koloskov A.V., Ponomarenko P.V., Tyrnov O.F. HF radar observations of decaying artificial field-aligned irregularities. *J. Geophys. Res*. 1996, vol. 101. P. 26981.

Kalishin A.S., Blagoveshchenskaya N.F., Borisova T.D., Rogov D.D. Remote diagnostics of effects induced by high-latitude heating facilities. *Russian Meteorology and Hydrology*. 2021, vol. 46, no. 4, pp. 231–240.

Kelley M.C. *The Earth's ionosphere: Plasma Physics and Electrodynamics.* San Diego. CA. USA: Academic Press. 1989, 556 p.

Koloskov A.V., Belei V.S., Leizer T.B., Yampolsky Yu.M. Radial drift of stimulated small-scale ionospheric irregularities perpendicular to the geomagnetic field. *Radiofizika i radioastronomiya* [Radiophysics and Radioastronomy]. 1999, vol. 4, no. 3, pp. 247–260. (In Russian).

Lester M., Chapman P.J., Cowley S.W.H., Crooks S.J., Davies J.A., Hamadyk P., et al. Stereo CUTLASS: A new

capability for the SuperDARN radars. *Ann. Geophys*. 2004, vol. 22, no. 2, pp. 459–473.

Myasnikov E.N., Muravjeva N.V., Sergeev E.N., Frolov V.L. Spatial spectrum of artificial ionospheric irregularities induced by powerful HF radio waves. *Radiophysics and Quantum Electronics*. 2001, vol. 44, no. 11, pp. 833–846.

Namazov S.A., Novikov V.D., Khmel'nitskii I.A. Doppler frequency shift during ionospheric propagation of decametric radio waves (Review). *Radiophysics and Quantum Electronics*. 1975, vol. 18, no. 4, pp. 345–364. DOI: 10.1007/BF01036419.

Nasyrov A.M. Scattering of Radio Waves by Anisotropic Ionospheric Irregularities. Kazan Univ. Publ., 1991, 149 p. (In Russian).

Rawer K., Bilitza D., Ramakrishnan S. Goals and Status of the International Reference Ionosphere. *Rev. Geophys*. 1978, vol. 16, no. 2, pp. 177–181. DOI: 10.1029/RG016i002p0017.

Rietveld M.T., Senior A., Markkanen J., Westman A. New capabilities of the upgraded EISCAT high-power HF facility. *Radio Sci*. 2016, vol. 51, no. 9, pp. 1533–1546. DOI: 10.1002/2016RS006093.

Rishbeth H., van Eyken A.P. EISCAT — early history and the first ten years of operation. *J. Atmos. Terr. Phys*. 1993, Vol. 55, no. 4-5. P. 525–542. DOI: 10.1016/0021-9169(93)90002-G.

Robinson T.R. The heating of the high latitude ionosphere by high power radio waves. *Phys. Rep*. 1989. Vol. 179, no. 2-3. P. 79–209. DOI: 10.1016/0370-1573(89)90005-7.

Sivokon V.P. A new method for research on magnetically oriented ionospheric inhomogeneities using a program of radio-system determination. *Geomagnetism and Aeronomy*. 2020, vol. 60, no. 2, pp. 236–242. DOI: 10.1134/s0016793220020140.

Stubbe P., Kopka H. Summary of results obtained with the Tromso heating facility. *Radio Sci*. 1983, vol. 18, no. 6, pp. 831–834. DOI: 10.1029/RS018i006p00831.

Thome G.D., Blood D.W. First observations of RF backscatter from field-aligned irregularities produced by ionospheric heating. *Radio Sci*. 1974, vol. 9, no. 11, P. 917–921. DOI: 10.1029/RS009i011p00917.

Uryadov V.P., Vertogradov G.G., Vertogradov V.G., Ponyatov A.A., Frolov V.L. Radar observations of artificial ionospheric turbulence during a magnetic storm. *Radiophysics and Quantum Electronics.* 2004, vol. 47, no. 9, pp.. 646–661.

Uryadov V.P., Ponyatov A.A., Vertogradov G.G., Vertogradov V.G., Kubatko S.V., Cherkashin Yu.N. Structure and dynamics of the ionospheric region with artificial small-scale irregularities according to complex measurements of the scattered radio-signal characteristics. *Radiophysics and Quantum Electronics*. 2009, vol. 51, no. 4, pp. 910–922**.**

Vas'kov V.V., Gurevich A.V. Nonlinear resonant instability of a plasma in the field of an ordinary electromagnetic wave. *JETP*. 1975, vol. 42, no. 1, p. 91.

Vas'kov V.V., Gurevich A.V. Self-focusing and resonant instability in ionospheric F region. *Thermal nonlinear plasma phenomena*. 1979, pp. 81–138. (In Russian).

Vertogradov G.G., Uryadov V.P., Vertogradov V.G., Vertogradova E.G., Kubatko S.V. Drift velocity of small-scale artificial ionospheric irregularities according to a multifrequency HF Doppler radar. II. Observation and modeling results. *Radiophysics and Quantum Electronics*. 2015, vol. 58, no. 11, pp. 381–389.

Yampolkii Yu.M. Echo scattering of SW signals by artificial ionospheric turbulence. *Radiofizika* [Radiophysics and Quantum Electronics]. 1989, vol. 32, no. 4, pp. 519–521. (In Russian).

Yampolski Y., Milikh G., Zalizovski A., Koloskov A., Reznichenko A., Nossa E., Bernhardt P.A., Briczinski S., Grach S.M., Shindin A., Sergeev E. Ionospheric Non-linear Effects Observed During Very-Long-Distance HF Propagation. *Front. Astron. Space Sci*. 2019, vol. 6, no. 12. DOI: 10.3389/ fspas.2019.00012.

Yeoman T.K., Wright D.M., Robinson T.R, Davies J.A., Rietveld M. High spatial and temporal resolution observations of an impulse-driven field line resonance in radar backscatter artificially generated with the Tromso heater. *Ann. Geophys*. 1997, vol. 1, no. 5, pp. 634–644. DOI: 10.1007/s00585-997-0634-9.

URL: https://flux.phys.uit.no/ArcMag/ (accessed April 3, 2024).

URL: https://rscf.ru/project/22-17-00020/ (accessed April 3, 2024).

Original Russian version: Borisova T.D., Blagoveshchenskaya N.F., Kalishin A.S., Kovalev A.S., published in Solnechno-zemnaya fizika. 2024. Vol. 10. Iss. 2. P. 79–98. DOI: 10.12737/szf-102202408.

How to cite this article

Borisova T.D., Blagoveshchenskaya N.F., Kalishin A.S., Kovalev A.S. Determination of the vector velocity of artificial ionospheric irregularities based on Doppler measurements by the bi-static scatter method of HF radio signals propagating over long radio paths. *Solar-Terrestrial Physics*. 2024. Vol. 10. Iss. 2. P. 74–92. DOI: 10.12737/stp-102202408.